Transient Acoustic Wave Propagation in Porous Media

Zine El Abiddine Fellah, Mohamed Fellah, Claude Depollier

Chapter 6

Transient Acoustic Wave Propagation in Porous Media

Zine El Abiddine Fellah, Mohamed Fellah and Claude Depollier

Additional information is available at the end of the chapter

http://dx.doi.org/10.5772/55048

1. Introduction

A porous material is a two-phase medium consisting of a solid part (skeleton) and a fluid part (pore space). During the propagation of a sound wave in such a medium, interactions between these two phases of different nature take place, giving various physical properties that are unusual in classical media. The large contact area between solid and fluid, which is the main characteristic of porous media induces new phenomena of diffusion and transport in the fluid, in relation to micro-geometry of the pore space. Many applications are concerned with understanding the behavior of acoustic waves in such media. In geophysics, we are interested in the propagation of acoustic waves in porous rocks, for information on soil composition and their fluid content. Oil companies have greatly contributed to the study of acoustic properties of natural porous media. In medicine, the characterization of porous media such as trabecular bone, is useful for diagnosing osteoporosis, bone disease that is manifested by the deterioration of bone microarchitecture. Acoustic characterization of materials is often achieved by measuring the attenuation coefficient and phase velocity in the frequency domain [1] or by solving the direct and inverse problems directly in the time domain [2–4]. The attractive feature of a time domain based approach is that the analysis is naturally limited by the finite duration of ultrasonic pressures and is consequently the most appropriate approach for the transient signal. The objective of this chapter is to show the most recent theoretical and experimental methods developed by the authors for the acoustic characterization of porous materials. The direct and inverse scattering problems are solved in time domain using experimental reflected and transmitted signals. The physical parameters of the porous medium are recovered by solving the inverse problem at the asymptotic domain corresponding to the high frequency range (ultrasound), and at the viscous domain (low frequency range). Figures 1 and 2 give an example of porous materials commonly used in the characterization. The figure 1 shows a sample of air-saturated plastic foam used for sound absorption, and figure 2 shows a sample of cancellous bone used in the diagnosis of the disease of osteoporosis.

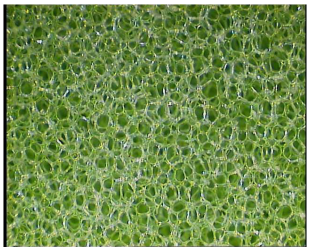

Figure 1. Air saturated Plastic foam

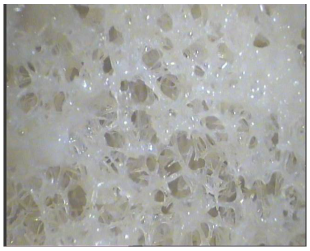

Figure 2. Human cancellous bone sample

2. Porous materials in rigid structure: Equivalent fluid model

2.1. Introduction

The air saturated porous materials are often used as a sound absorber in the fight against noise pollution. The polyurethane foam, felt or glass wools are three examples of common materials used in aerospace and automotive industries and in building construction. Generally, when a sound wave propagates through a porous material saturated with air, the structure remains stationary and non-deformable with respect to the acoustic excitation, this is due to the heaviness and stiffness of the skeleton of the structure relative in air. This is called porous rigid structure and, in this case, we use the equivalent fluid model where viscous and thermal effects are disconnected [5]. The fluid-structure interactions responsible for the sound attenuation (particularly important in porous media), are described by two dynamic susceptibilities, the dynamic tortuosity and compressibility. The dynamic tortuosity [6] decribes the viscous and inertial effects, the dynamic compressibility [7–9] represents the thermal effects. A prediction of the acoustic behavior of porous material requires the determination of both dynamic susceptibilities. The latter can depend only on the physical characteristics of the fluid and the geometry of the fluid domain. Sound propagation in the saturating fluid involves both transport and diffusion characteristics. The phenomenon of transport is the fact that a global movement fluid/solid is induced during the propagation. The phenomenon of diffusion is related to the expansion/compression of the fluid. They result in a change in temperature fluid/solid (the latter remaining at room temperature) driving a heat diffusion, not negligible if the fluid is a gas. Moreover, in the case of sound propagation, the frequency of movement is important. It is clear that the character of the movement is changed to different frequencies, the fluid probe different aspects of micro geometry. In principle one should expect that there are an infinite number of geometric parameters. But on the other hand, a practical viewpoint, the information provided by a

finite set of parameters low and high frequencies may be sufficient to describe the dynamic susceptibilities. For a given frequency, one can define a boundary layer thickness, respectively viscous and thermal $\delta = (2\eta/\omega\rho_f)^{1/2}$, $\delta' = (2\kappa/\rho_f C_p\omega)^{1/2}$, where η is the viscosity, ρ_f the fluid density, κ the coefficient of thermal conduction, C_p the specific heat at constant pressure and ω the angular frequency. The quantities δ and δ' are respectively the penetration depths of isothermal viscous and rotational movement. The boundary layer is small if the penetration depth is small compared to a "radius" characteristic pore. It is then at high frequencies. The opposite situation corresponds to low frequencies. In the high frequencies, inertial effects are described by the tortuosity α_∞, the visco-thermal losses by viscous and thermal lengths Λ et Λ', respectively. At low frequencies, inertial effects are represented by the viscous tortuosity α_0, and visco-thermal exchanges by the visco-thermal permeabilities k_0 and k'_0. Porosity ϕ is a parameter playing an important role both in high in low frequency.

2.2. Parameters describing the porous materials

There are several geometrical parameters that can be associated with a porous structure. Some depend only on the shape of the porous solid and do not vary when it expands or changes the scale of the solid. This is the case of the porosity and tortuosity. Others depend on the dimensions, in the case of viscous and thermal permeabilities that vary in shape as an equal surface, and viscous and thermal characteristic lengths that vary as lengths.

- **Porosity** ϕ: The porosity of a porous material saturated with a fluid is defined by the ratio of the volume of fluid saturating the porous medium to the total volume of the sample. This quantity is dimensionless and can vary from 0 (non-porous solid material) to 1 (free fluid).
- **Tortuosity** α_∞: The tortuosity is a geometric parameter describing the appearance of tortuous pores, and inertial coupling between the fluid and the structure of the material in high-frequency regime. Tortuosity takes its lowest value ($\alpha_\infty = 1$) in the case of porous materials having a straight pores, and large values (α_∞ = 1.5, 2) for the most resistive material.
- **Inertial factor** α_0 **(low frequency tortuosity)**: The inertial factor α_0 corresponds to the low frequency approximation of the dynamic tortuosity given by Norris [10]; $\alpha_0 = \frac{<\mathbf{v}(\mathbf{r})^2>}{<\mathbf{v}(\mathbf{r})>^2}$, where $< \mathbf{v}(\mathbf{r}) >$ is the average velocity of the viscous fluid for direct current flow within an elementary volume, small compared to the relevant wavelength, but large compared to the individual grains/pores of the solid. Note that the tortuosity α_∞ (high frequency parameter) has a similar definition than α_0, the difference is that for α_∞, $\mathbf{v}(\mathbf{r})$ corresponds to the velocity of the perfect incompressible fluid.
- **Thermal tortuosity** α'_0: This low frequency parameter is the thermal counterpart of α_0. Its definition is given by: $\alpha'_0 = \frac{<\theta_0^2>}{<\theta_0>^2}$, where θ_0 is the scaled response excess temperature field in the low frequency range.
- **The specific flow resistivity** σ: When a porous material placed in a tube sealed to the walls, is traversed by a fluid, it is a pressure difference between the two free faces. This means that a proportional relationship exists between flow rate Q_v and pressure drop ΔP given by the $\Delta P = RQ_v$, the coefficient R is the resistance to fluid flow and can therefore be defined as the ratio $\Delta P/Q_v$. For a homogeneous porous material, the resistance is proportional to

the length d of the sample and inversely to his section S. Then can be defined, the resistivity as the specific resistance to the passage of a fluid. Denoted σ, the resistivity is defined by $\sigma = (S/d)R$.

- **Viscous permeability** k_0: Static viscous permeability is related to the flow resistivity by the relation $k_0 = \eta/\sigma$, where η is the dynamic viscosity of the fluid. Viscous permeability is a geometrical parameter, homogeneous to a surface (it is expressed in m^2), independent of the nature of the saturating fluid and depending only on the internal geometry of the porous material. This parameter represents the effective pore section for the flow of fluid, it is connected to the low frequency behavior of the fluid exchange between viscous and saturating the porous structure.
- **Viscous characteristic length** Λ: The work of Johnson et al [6] in 1987 on the characterization of viscous effects at high frequencies has introduced the viscous characteristic length Λ given by $\frac{2}{\Lambda} = \frac{\int_S u^2 dS}{\int_V u^2 dV}$ where u is the speed of a microscopic incompressible perfect fluid, S the area of the interface between solid and fluid phases and V the volume of fluid. The length Λ is a geometrical parameter. This definition applies to a smooth interface fluid/solid, and for a low boundary layer thickness to the radius of curvature characteristic of the interface. When the pore surface has singularities (peaks), this definition of the characteristic length is no longer valid. The parameter Λ is an indicator of the size of the narrow neck of the pore, i.e. the privileged place of viscous exchanges.
- **Thermal characteristic length** Λ': In 1991, Allard and Champoux [8], introduced by analogy with Johnson *et al* [6], a geometric parameter called thermal characteristic length given by $\frac{2}{\Lambda'} = \frac{\int_S dS}{\int_V dV}$. In other words Λ' is twice the ratio of fluid volume on the total contact surface between the solid and fluid. The factor 2 is introduced so that in the case of cylindrical pores, Λ' is the pore radius. The length Λ' is an indicator of the size of large pores, privileged place of heat exchange.
- **Thermal permeability** k'_0: The study of viscous and thermal effects shows that there are similarities between these two effects. Starting from the equation of heat diffusion, Lafarge [9] introduced the equivalent of Darcy's law for the temperature excess, by introducing a new parameter: the thermal permeability k'_0, which is the inverse of the constant trapping.

2.3. Models of dynamic susceptibilities

There are several models describing the inertial viscous and thermal exchanges between the fluid and the structure. We present here the most elaborate.

2.3.1. The model of Johnson et al. for the dynamic tortuosity

Johnson et al [6] have proposed a simple model describing the function $\alpha(\omega)$, which is the dynamic tortuosity, when the porous structure is saturated with a Newtonian viscous fluid. This model can be applied to the case of our porous structures saturated with air. Two model parameters, the tortuosity α_∞ and the viscous characteristic length Λ are involved in a high-frequency limit:

$$\alpha(\omega) = \alpha_\infty \left(1 - \frac{2}{\Lambda}\left(\frac{\eta}{j\omega\rho_f}\right)^{1/2}\right), \qquad \omega \longrightarrow \infty. \tag{1}$$

where $j^2 = -1$, η is the dynamic viscosity of the fluid, ω the angular frequency, ρ_f the density of the fluid. In the low frequency limit, the expression of the dynamic tortuosity in the frequency domain is given by:

$$\alpha(\omega) = -\frac{\eta\phi}{\rho_f k_0 j\omega}, \qquad \omega \longrightarrow 0, \tag{2}$$

where, k_0 is the viscous permeability given by: $k_0 = \frac{\eta}{\sigma}$ (with the dimension of a surface), σ is the specific resistance passage of the fluid. The meaning of the quantities α_∞, Λ, k_0 have been given previously. Johnson et al [6] imply that these three geometric parameters provide sufficient information about the microgeometry. The proposed general expression for $\alpha(\omega)$ is then that of the simplest analytic function verifying these limits:

$$\alpha(\omega) = \alpha_\infty \left(1 - \frac{1}{jx}\sqrt{1 - \frac{M}{2} j\, x}\right) \quad \text{where} \quad x = \frac{\omega\alpha_\infty\rho_f}{\sigma\phi} \quad \text{and} \quad M = \frac{8k_0\alpha_\infty}{\phi\Lambda^2}. \tag{3}$$

2.3.2. The equivalent model for the dynamic compressibility

A model similar to the previous one has been set for the frequency dependence of the thermal exchanges between the fluid and the structure, because of the heat capacity of the solid part is significant. The result is a two-parameter model, Λ' and k_0'/ϕ, the quantities Λ' and k_0'/ϕ for thermal effects playing respectively the role of Λ and k_0 for viscous effects. In a high-frequency limit, Allard and Champoux [7, 8] showed the following behavior of $\beta(\omega)$:

$$\beta(\omega) = 1 - \frac{2(\gamma-1)}{\Lambda'}\left(\frac{\eta}{P_r\rho_f}\right)^{1/2}\left(\frac{1}{j\omega}\right)^{1/2}, \qquad \omega \longrightarrow \infty, \tag{4}$$

where Pr is the number of Prandt and γ the adiabatic constant. As before, this behavior implies that the thermal boundary layer thickness δ' becomes small compared to any characteristic radius of curvature of the interface. One can see that there is no equivalent of the tortuosity α_∞ for thermal effects, at very high frequency $\beta(\omega)$ tends to 1 as $\alpha(\omega)$ tends to the tortuosity α_∞.

In a low frequency limit, Lafarge [9] showed that:

$$\beta(\omega) = \gamma + \frac{(\gamma-1)\rho_f k_0' P_r}{\eta\phi\, j\omega}, \qquad \text{when} \qquad \omega \longrightarrow 0. \tag{5}$$

where k_0', which has the same size (area) that the Darcy permeability of k_0, is a parameter analogous to the parameter k_0, but adapted to the thermal problem. The proposed general expression for $\beta(\omega)$ is then that of the simplest analytic function satisfying the limits ((4) and (5):

$$\beta(\omega) = \gamma - (\gamma-1)/\left[1 - \frac{1}{j\,x'}\sqrt{1 - \frac{M'}{2} j\, x'}\right] \quad \text{where} \quad x' = \frac{\omega\rho_f k_0' P_r}{\eta\phi} \quad \text{and} \quad M' = \frac{8k_0'}{\phi\Lambda'^2}.$$

the parameter k_0' introduced by Lafarge called thermal permeability by analogy to the viscous permeability.

2.3.3. Extensions of models by pride and Lafarge

The development of Johnson et al in high frequency for the tortuosity dynamics stops after the term $\frac{1}{\sqrt{j\omega}}$, Pride *et al* [11] proposed a second correction term which is $\frac{1}{j\omega}$. The asymptotic expansion of the dynamic tortuosity now is written as follows:

$$\alpha(\omega) = \alpha_\infty \left(1 - \frac{2}{\Lambda}\left(\frac{\eta}{j\omega\rho_f}\right)^{1/2} - \frac{\sigma\phi(1-\wp)}{j\omega\rho_f\alpha_\infty}\right), \qquad \omega \longrightarrow \infty. \tag{6}$$

The Pride parameter $\wp$ [11] is a geometrical parameter, dimensionless, connected to a correction term α_0 playing the role of inertia of fluid at low frequencies:

$$\wp = \frac{M}{4\left(\frac{\alpha_0}{\alpha_\infty} - 1\right)}, \qquad \text{where} \qquad M = \frac{8k_0\alpha_\infty}{\phi\Lambda^2}.$$

The expansion of low frequency dynamic tortuosity is given by:

$$\alpha(\omega) = -\frac{\eta\phi}{\rho_f k_0 j\omega} + \alpha_0, \qquad \omega \longrightarrow 0 \tag{7}$$

The new expression of the analytic function taking into account developments of (6) and (7) is given by:

$$\alpha(\omega) = \alpha_\infty \left(1 - \frac{1}{jx}\left(1 - \wp + \wp\sqrt{1 - \frac{M}{2\wp^2}jx}\right)\right).$$

The value of $\wp$ depends on the geometry of the pores, for example in the case of cylindrical pores of circular section, it is shown that $\wp = 3/4$. For rectangular sections, one obtains values close to 3/4.

For thermal effects, Lafarge [9] suggested a similar expression for the dynamic thermal compressibility, also introducing a dimensionless parameter $\wp'$ and gives a correction to the Allard and Champoux model at high frequencies. The expression of the dynamic compressibility is then given by:

$$\beta(\omega)=1-(\gamma-1)\left[\frac{2}{\Lambda'}\left(\frac{\eta}{P_r\rho_f}\right)^{1/2}\left(\frac{1}{j\omega}\right)^{1/2}+\left(\frac{\eta}{\rho_f P_r j\omega}\right)\cdot\left(\frac{(1-\wp')\phi}{k_0'}-\frac{4}{\Lambda'^2}\right)\right], \omega \longrightarrow \infty. \tag{8}$$

The parameter $\wp'$ is connected to α_0', thermal equivalent of α_0, which describes the thermal inertia of fluid at low frequency:

$$\wp' = \frac{M'}{4(\alpha_0' - 1)}.$$

The general expression for the dynamic compressibility is then given by:

$$\beta(\omega) = \gamma - (\gamma - 1)/\left[1 - \frac{1}{jx'}\left(1 - \wp' + \wp'\sqrt{1 - \frac{M'}{2\wp'^2}jx'}\right)\right].$$

One can notice that the models of Pride and Lafarge are reduced to those of Johnson and Allard when $\wp = 1$ and $\wp' = 1$. We will see later the influence of these parameters on the propagation.

2.4. Temporal modeling of propagation: asymptotic regime

The use of transient signals in the acoustic characterization of porous media is widely used experimentally. These signals have a wide frequency content making some complicated frequency approaches. The frequency methods are very effective for monochromatic signals, however, for transient signals, the temporal approach [2, 12–15] is best suited for several reasons:

- Time domain analysis is naturally bounded (limited) by the finite duration of impulses.
- Time-modeling is often easier to develop because it is closer to the reality of experiments.
- In many situations, the introduction of the "time" parameter make easier the analysis of experimental results.
- For certain applications, it is fast because it avoids back and forth operations between time and frequency domains by FFT.
- It provides an elegant solution of the direct problem necessary for the resolution of the inverse problem.
- It is well suited for comparison between theory and experiment.

In return for these benefits, it is necessary to use a new mathematical formalism. In the frequency domain approach, the relevant quantities for the characterization of porous media are functions of frequency which can be interpreted as susceptibilities. While frequency methods lead to the frequency responses of the medium, in the temporal approach, one is interested in these impulse responses.

2.5. Concept of fractional derivative and propagation equation

In the asymptotic regime corresponding to high frequencies, the fluid-structure interactions are described by expressions (1) et (4) according to the Johnson-Allard model. Writing the equations in the time domain is equivalent to taking the inverse Fourier transform of (1) and (4). The temporal equivalent of $j\omega$ is $\partial/\partial t$, while the temporal equivalent of $\sqrt{j\omega}$ is a fraction0al derivative of order $1/2$. The definition of fractional derivative of order ν is given by [16]:

$$D^{\nu}[x(t)] = \frac{1}{\Gamma(-\nu)} \int_0^t (t-u)^{-\nu-1} x(u)du, \tag{9}$$

where Γ is the Eulerian function of the second kind [17]. From the definition (9), the expressions of response factors $\alpha(\omega)$ and $\beta(\omega)$ are then given in the time domain by [2]:

$$\alpha(\omega) \xrightarrow{t} \alpha_\infty \delta(t) + \frac{1}{\rho_f}\chi_v(t),$$

$$\beta(\omega) \xrightarrow{t} \delta(t) + K_a \chi_{th}(t),$$

where $\delta(t)$ is the Dirac distribution and the operators, K_a the modulus of the fluid, $\chi_v(t)$ and $\chi_{th}(t)$ are given by:

$$\chi_v(t) = \frac{2\rho_f \alpha_\infty}{\Lambda}\sqrt{\frac{\eta}{\pi\rho_f}}\, t^{-1/2},$$
$$\chi_{th}(t) = \frac{2(\gamma-1)}{K_a\Lambda'}\sqrt{\frac{\eta}{\pi P_r \rho_f}}\, t^{-1/2},$$

In this model, the time convolution of $t^{-1/2}$ with a function, is interpreted as an operator of fractional derivative. The acoustic fields satisfy the Euler equation and the constitutive equation [2] given by:

$$\rho_f \alpha_\infty\, \partial_t \mathbf{v}(\mathbf{r},t) + \int_0^t \chi_v(t-t')\, \partial_t \mathbf{v}(\mathbf{r},t')\, dt' = -\nabla p(\mathbf{r},t), \tag{10}$$
$$\frac{1}{K_a}\, \partial_t p(\mathbf{r},t) + \int_0^t \chi_{th}(t-t')\, \partial_t p(\mathbf{r},t')\, dt' = -\nabla.\mathbf{v}(\mathbf{r},t). \tag{11}$$

These constitutive relations in the time domain satisfy the principle of causality. In these equations, p is the acoustic pressure, $\mathbf{v}$ the particle velocity. The term $\alpha_\infty\delta(t)$ reflects the instantaneous response of the porous medium and describes the inertial coupling between fluid and structure. For instantaneous responses, we mean that the time response is smaller than the characteristic time scale of the change in the acoustic field. The susceptibilities χ_v and χ_{th} are operators of memory that determine the dispersion of the medium.

We assume that the medium varies with the thickness x only, and that the incident wave is plane and normal to the surface of the material. Sound pressure is denoted by $p(x,t)$. We assume that the pressure field is zero for moments earlier to 0. The wave equation for acoustic pressure field of a porous medium having a dispersive rigid structure is obtained from the constitutive equations (10, 11), and is of the form:

$$\partial_x^2 p(x,t) - \frac{1}{c_0^2}\left[\alpha_\infty \partial_t^2 p(x,t) + \left(\alpha_\infty K_a \chi_{th} + \frac{\chi_v}{\rho_f} + c_0^2 \chi_{th} * \chi_v\right) * \partial_t^2 p(x,t)\right] = 0, \tag{12}$$

where $c_0 = (K_a/\rho_f)^{1/2}$ is the sound speed in the free fluid. The following notation is used for convolution integrals of two causal functions $f(x,t)$ and $g(x,t)$;

$$[f * g](x,t) = \int_0^t f(x,t-t')g(x,t')dt'.$$

The propagation equation (12) can be written as:

$$\frac{\partial^2 p(x,t)}{\partial x^2} - A\frac{\partial^2 p(x,t)}{\partial t^2} - B\int_0^t \frac{\partial^2 p(x,t)/\partial t'^2}{\sqrt{t-t'}}dt' - C\frac{\partial p(x,t)}{\partial t} = 0, \tag{13}$$

where the coefficients A, B and C are constant and given by:

$$A = \frac{\rho_f \alpha_\infty}{K_a}, \quad B = \frac{2\alpha_\infty}{K_a}\sqrt{\frac{\rho_f \eta}{\pi}}\left(\frac{1}{\Lambda} + \frac{\gamma-1}{\sqrt{Pr}\Lambda'}\right) \quad C = \frac{4\alpha_\infty(\gamma-1)\eta}{K_a\Lambda\Lambda'\sqrt{Pr}},$$

respectively, The coefficient A gives the wave velocity $c = 1/\sqrt{\rho_f \alpha_\infty / K_a}$ in the air saturating the porous medium. α_∞ plays the role of the refractive index of the porous medium that changes the speed $c_0 = \sqrt{K_a/\rho_f}$ in free space to $c_0 = c/\sqrt{\alpha_\infty}$ in the porous medium. The other coefficients depend essentially on characteristic lengths Λ and Λ' and express the fluid-structure visco-thermal interactions. The constant B describes the dispersion of the signal and C the attenuation of the amplitude of the wave (without dispersion). The propagation equation (13) describes the evolution of the acoustic wave inside the porous material. The boundary conditions have not been introduced, the porous medium is assumed to be infinite. The coefficients of the equation of propagation do not depend on the porosity, in fact, porosity appears at the interfaces of the porous material via the relationship of continuity of acoustic flow (the flow rate is equal to the porosity multiplied by the speed). This parameter appears naturally at the reflection and transmission of an acoustic wave through a slice of porous material. The solution of the wave equation (13) is given by the Green function G of the porous medium [3, 18], defined by:

$$p(x,t) = \int_0^t G(x, t-t')p(0,t)dt',$$

where $p(x,t)$ is the sound pressure in the porous medium and $p(0,t)$ the incident signal.

2.6. Solution of the propagation equation: Green function (Johnson-Allard model)

To solve the propagation equation and obtain the Green function of the medium, we solve the equation (13) using the method of Laplace transform [18], taking into account the following initial conditions of causality:

$$p(x,t)|_{t=0} = 0 \quad \text{and} \quad \frac{\partial p}{\partial t}|_{t=0} = 0. \tag{14}$$

Denote by $P(x,z)$ the Laplace transform of $p(x,t)$ defined by:

$$P(x,z) = \mathcal{L}\left[p(x,t)\right] = \int_0^\infty \exp(-zt)p(x,t)dt,$$

and the inverse Laplace transform by:

$$p(x,t) = \mathcal{L}^{-1}\left[P(x,z)\right].$$

Using the following relationship:

$$\mathcal{L}\left[\delta(t)\right] = 1, \qquad \mathcal{L}\left[H(t)\right] = \frac{1}{z} \qquad \text{and} \qquad \mathcal{L}\left[\frac{1}{\sqrt{t}}\right] = \sqrt{\frac{\pi}{z}},$$

where $H(t)$ is the Heaviside jump function, the Laplace transform of the wave equation (13) is:

$$\frac{\partial^2 P(x,z)}{\partial x^2} - z^2\left(\frac{1}{c^2} + \frac{C}{z} + B\sqrt{\frac{\pi}{z}}\right)P(x,z) = -\left(\frac{1}{c^2} + B\sqrt{\frac{\pi}{z}}\right)\left(zp(x,0) + \frac{\partial p(x,0)}{\partial t}\right) - Cp(x,0). \tag{15}$$

Taking into account the initial conditions (14), equation (15) simplifies to

$$\frac{\partial^2 P(x,z)}{\partial x^2} - z^2\left(\frac{1}{c^2} + \frac{C}{z} + B\sqrt{\frac{\pi}{z}}\right)P(x,z) = 0,$$

which is a second order differential equation with real coefficients constant. The general solution of equation is:

$$P(x,z) = e^{-\frac{x}{c}\sqrt{f(z)}}\varphi(z) + e^{\frac{x}{c}\sqrt{f(z)}}\psi(z),$$

where $\varphi(z)$ and $\psi(z)$ are two independent functions of x and:

$$f(z) = z^2\left(1 + \frac{Cc^2}{z} + Bc^2\sqrt{\frac{\pi}{z}}\right) = z(z + b'\sqrt{z} + c'). \tag{16}$$

In equation (16), the constants b' and c' are positive and are given by:

$$b' = Bc^2\sqrt{\pi} \quad \text{and} \quad c' = Cc^2. \tag{17}$$

Retaining the finite solution at infinity, which corresponds to the physical solution of our problem, we have:

$$P(x,z) = e^{-\frac{x}{c}\sqrt{f(z)}}\varphi(z).$$

The solution of equation (13) is the inverse Laplace transform of $P(x,z)$. We obtain:

$$p(x,t) = \mathcal{L}^{-1}\left(e^{-\frac{x}{c}\sqrt{f(z)}}\varphi(z)\right) = \mathcal{L}^{-1}\left(e^{-\frac{x}{c}\sqrt{f(z)}}\right) * \mathcal{L}^{-1}\left(\varphi(z)\right).$$

The core problem is the calculation of the inverse Laplace transform of the term $\mathcal{L}^{-1}\left(e^{-\frac{x}{c}\sqrt{f(z)}}\right)$. This has been well studied in reference [18]. By letting:

$$\Delta^2 = b'^2 - 4c', \tag{18}$$

it is easy to check that Δ^2 is always positive in the Johnson-Allard model. The expression of $f(z)$ (Eq. 16) can be written as

$$f(z) = \left(z + \frac{b'}{2}\sqrt{z}\right)^2 - \left(\frac{\Delta\sqrt{z}}{2}\right)^2. \tag{19}$$

When $\Delta = 0$, the solution of the propagation equation(13) is given [18] by:

$$p(x,t) = \begin{cases} 0, & \text{if} \quad 0 \le t \le x/c, \\ \frac{1}{4\sqrt{\pi}}\frac{b'x}{c}\int_{x/c}^{t}\frac{1}{(\tau - x/c)^{3/2}}\exp\left(-\frac{b'^2x^2}{16c^2(\tau - x/c)}\right)p(0,t-\tau)d\tau, & \text{if} \quad t > x/c, \end{cases} \tag{20}$$

where $p(0,t) = \mathcal{L}^{-1}\left(\varphi(z)\right)$. In this case the Green function is given [18, 19] by:

$$G(x,t) = \begin{cases} 0, & \text{if} \quad 0 \le t \le x/c, \\ \frac{1}{4\sqrt{\pi}}\frac{b'x}{c}\frac{1}{(t - x/c)^{3/2}}\exp\left(-\frac{b'^2x^2}{16c^2(t - x/c)}\right), & \text{if} \quad t > x/c, \end{cases} \tag{21}$$

When $\Delta^2 > 0$, the general solution of the propagation equation is given by:

$$p(x,t)=\begin{cases} 0, & \text{if} \quad 0 \le t \le x/c, \\ \frac{x}{c}\int_{x/c}^{t}\left(\frac{b'}{4\sqrt{\pi}}\frac{1}{(\tau-x/c)^{3/2}}\exp\left(-\frac{b'^2x^2}{16c^2(\tau-x/c)}\right)+\Delta\int_0^{\tau-x/c}h'(\xi)d\xi\right)p(0,t-\tau)d\tau, & t > x/c. \end{cases} \tag{22}$$

where

$$h'(\xi) = -\frac{1}{4\pi^{3/2}}\frac{1}{\sqrt{(\tau-\xi)^2-x^2/c^2}}\frac{1}{\xi^{3/2}}\int_{-1}^{1}\exp\left(-\frac{\left(\mu\Delta\sqrt{(\tau-\xi)^2-x^2/c^2}+b'(\tau-\xi)\right)^2}{16\xi}\right)$$
$$\times\left(\frac{\left(\mu\Delta\sqrt{(\tau-\xi)^2-x^2/c^2}+b'(\tau-\xi)\right)^2}{8\xi}-1\right)\frac{\mu d\mu}{\sqrt{1-\mu^2}}.$$

In this case, the Green function [18] is given by:

$$G(x,t) = \begin{cases} 0, & \text{if} \quad 0 \le t \le x/c, \\ \frac{x}{c}\left(\frac{b'}{4\sqrt{\pi}}\frac{1}{(t-x/c)^{3/2}}\exp\left(-\frac{b'^2x^2}{16c^2(t-x/c)}\right)+\Delta\int_0^{t-x/c}h'(\xi)d\xi\right), & \text{if} \quad t > x/c. \end{cases} \tag{23}$$

2.7. Solution of the propagation equation: Green function (Pride-Lafarge model)

Extensions of Pride-Lafarge (6,8) are expressed in the time domain [3] using the definition of fractional derivative:

$$\tilde{\alpha}(t) = \alpha_\infty\left(\delta(t)+\frac{2}{\Lambda}\left(\frac{\eta}{\rho_f}\right)^{1/2}\frac{\partial^{-1/2}}{\partial t^{-1/2}}+\frac{\sigma\phi(1-\wp)}{\rho_f\alpha_\infty}\frac{\partial^{-1}}{\partial t^{-1}}\right),$$

$$\tilde{\beta}(t) = \delta(t)+(\gamma-1)\left(\frac{2}{\Lambda'}\left(\frac{\eta}{P_r\rho_f}\right)^{1/2}\frac{\partial^{-1/2}}{\partial t^{-1/2}}+\left(\frac{\eta}{\rho_f P_r}\right)\left[\frac{(1-\wp')\phi}{k_0'}-\frac{4}{\Lambda'^2}\right]\frac{\partial^{-1}}{\partial t^{-1}}\right),$$

$\tilde{\alpha}(t)$ and $\tilde{\beta}(t)$ are the operators of tortuosity and compressibility. In these equations, the operator $\partial^{-1}/\partial t^{-1}$ represents the time integral:

$$\frac{\partial^{-1}x(t)}{\partial t^{-1}} = \int_0^t x(t')dt',$$

and semi-operator $\partial^{-1/2}/\partial t^{-1/2}$ represents the fractional derivative. In this case, the basic equations are given by:

$$\rho_f\alpha_\infty\,\partial_t\mathbf{v}(\mathbf{r},t)+\int_0^t\chi_v'(t-t')\,\partial_t\mathbf{v}(\mathbf{r},t')\,dt' = -\nabla p(\mathbf{r},t), \tag{24}$$

$$\frac{1}{K_a}\,\partial_t p(\mathbf{r},t)+\int_0^t\chi_{th}'(t-t')\,\partial_t p(\mathbf{r},t')\,dt' = -\nabla.\mathbf{v}(\mathbf{r},t), \tag{25}$$

where the operators $\chi'_v(t)$ and $\chi'_{th}(t)$ are given by:

$$\chi'_v(t) = \frac{2\rho_f \alpha_\infty}{\Lambda}\sqrt{\frac{\eta}{\pi\rho_f}}\, t^{-1/2} + \sigma\phi(1-\wp)\frac{\partial^{-1}}{\partial t^{-1}},$$

$$\chi'_{th}(t) = \frac{2(\gamma-1)}{K_a\Lambda'}\sqrt{\frac{\eta}{\pi P_r\rho_f}}\, t^{-1/2} + \left(\frac{\eta(\gamma-1)}{K_a\rho_f P_r}\right)\left[\frac{(1-\wp')\phi}{k'_0} - \frac{4}{\Lambda'^2}\right]\frac{\partial^{-1}}{\partial t^{-1}},$$

In these expressions, the convolutions express the dispersive nature of the porous material. They take into account the memory effect, where the medium response to excitation of the wave is not instantaneous but takes some time.

The propagation equation can be easily obtained from (24, 25). The propagation equation obtained has exactly the same form as the equation (13), the only difference appears at the coefficient $C = \left(\frac{4\alpha_\infty(\gamma-1)\eta}{K_a\Lambda\Lambda'\sqrt{P_r}} + \frac{\sigma\phi(1-\wp)}{K_a} + \frac{\alpha_\infty(\gamma-1)\eta}{K_a k'_0 P_r}\left[\frac{(1-\wp')\phi}{k'_0} - \frac{4}{\Lambda'^2}\right]\right)$, However, we will see that its solution is different. Since the coefficient C exchange rate, the coefficients c' and Δ given by equation ((17, 18) also change. With extensions of Pride-Lafarge, the coefficient Δ^2 can be negative [3], it gives:

$$\Delta'^2 = -\Delta^2 \Longrightarrow \Delta'^2 = 4c' - b'^2. \tag{26}$$

In this case, $f(z)$ given by equation (16) can be written in the form:

$$f(z) = \left(z + \frac{b'}{2}\sqrt{z}\right)^2 + \left(\frac{\Delta'\sqrt{z}}{2}\right)^2. \tag{27}$$

Using expressions (26 and 27) and analytical calculations given in [3], we obtain the solution of the wave equation when Δ^2 is negative:

$$p(x,t) = \begin{cases} 0, & \text{if} \quad 0 \le t \le x/c, \\ \int_{x/c}^{t}\left[F_1(\tau) + \int_0^{\tau-x/c} H(\xi,\tau)d\xi + j\int_0^{\tau-x/c}\Xi(\xi,\tau)d\xi\right] p(0,t-\tau)d\tau & \text{if} \quad t > x/c. \end{cases} \tag{28}$$

with

$$F_1(\tau) = \frac{1}{4\sqrt{\pi}} b' \frac{x}{c}\frac{1}{(\tau - x/c)^{3/2}}\exp\left(-\frac{b'^2x^2}{16c^2(\tau - x/c)}\right), \quad j^2 = -1.$$

The functions $H(\xi,\tau)$ and $\Xi(\xi,\tau)$ are given by the following equations where τ is replaced by t:

$$H(\xi,t) = \frac{\Delta'}{4\pi\sqrt{\pi}}\frac{x}{c}\frac{1}{\sqrt{(t-\xi)^2 - x^2/c^2}}\frac{1}{\xi^{3/2}} \times$$
$$\int_{-1}^{1}\left[\frac{\mathcal{A}\mathcal{B}}{4\xi}\cos\left(\frac{\mathcal{A}\mathcal{B}}{8\xi}\right) - \left(\frac{\mathcal{B}^2 - \mathcal{A}^2}{8\xi} - 1\right)\sin\left(\frac{\mathcal{A}\mathcal{B}}{8\xi}\right)\right]\exp\left(-\frac{\mathcal{B}^2 - \mathcal{A}^2}{16\xi}\right)\frac{\mu d\mu}{\sqrt{1-\mu^2}}$$

and

$$\Xi(\xi,t) = -\frac{\Delta'}{4\pi\sqrt{\pi}}\frac{x}{c}\frac{1}{\sqrt{(t-\xi)^2 - x^2/c^2}}\frac{1}{\xi^{3/2}}$$
$$\int_{-1}^{1}\left[\left(\frac{\mathcal{B}^2 - \mathcal{A}^2}{8\xi} - 1\right)\cos\left(\frac{\mathcal{A}\mathcal{B}}{8\xi}\right) + \frac{\mathcal{A}\mathcal{B}}{4\xi}\sin\left(\frac{\mathcal{A}\mathcal{B}}{8\xi}\right)\right]\exp\left(-\frac{\mathcal{B}^2 - \mathcal{A}^2}{16\xi}\right)\frac{\mu d\mu}{\sqrt{1-\mu^2}},$$

where

$$\mathcal{A} = \Delta' \mu \sqrt{(t-\xi)^2 - x^2/c^2} \qquad \text{and} \qquad \mathcal{B} = b'(t-\xi).$$

The Green function is given by [3]:

$$G(t,x) = \begin{cases} 0, & \text{if} \quad 0 \le t \le x/c, \\ F_1(t) + \int_0^{t-x/c} H(\xi,t)d\xi + j\int_0^{t-x/c} \Xi(\xi,t)d\xi \qquad \text{if} & t > x/c. \end{cases} \tag{29}$$

2.8. The reflection and transmission operators

For a slice of porous material occupying the domain $0 \le x \le L$, the incident and scattered fields are connected by scattering operators (i.e. operators of reflection and transmission) of the material. These are operators [4] represented in integral form:

$$p^r(x,t) = \int_0^t \tilde{R}(\tau) p^i\left(t - \tau + \frac{x}{c_0}\right) d\tau, \tag{30}$$

$$p^t(x,t) = \int_0^t \tilde{T}(\tau) p^i\left(t - \tau - \frac{L}{c} - \frac{(x-L)}{c_0}\right) d\tau. \tag{31}$$

In equations (30) and (31) functions $\tilde{R}$ and $\tilde{T}$ represent the kernel of reflection and transmission operators, respectively. These are independently-owned operators of the incident field and depend only on the material properties. To express the operators of reflection and transmission, we assume [4] that the field of acoustic pressure and flow are continuous at the interfaces of the material:

$$\begin{aligned} p(0^+,t) &= p(0^-,t), & p(L^-,t) &= p(L^+,t) \\ v(0^-,t) &= \phi v(0^+,t), & v(L^+,t) &= \phi v(L^-,t) \end{aligned} \tag{32}$$

The expressions of $\tilde{R}$ and $\tilde{T}$ are given by (see Ref. [4])

$$\tilde{R}(t) = \left(\frac{-\phi + \sqrt{\alpha_\infty}}{\phi + \sqrt{\alpha_\infty}}\right) \sum_{n\ge 0} \left(\frac{\phi - \sqrt{\alpha_\infty}}{\phi + \sqrt{\alpha_\infty}}\right)^{2n} \left[G\left(t, 2n\frac{L}{c}\right) - G\left(t, (2n+2)\frac{L}{c}\right)\right],$$

$$\tilde{T}(t) = \frac{4\phi\sqrt{\alpha_\infty}}{\left(\sqrt{\alpha_\infty} + \phi\right)^2} \sum_{n\ge 0} \left(\frac{\phi - \sqrt{\alpha_\infty}}{\phi + \sqrt{\alpha_\infty}}\right)^{2n} G\left(t + \frac{L}{c_0}, (2n+1)\frac{L}{c}\right).$$

where G is the Green function of the medium. These expressions take into account the multiple n reflections within the porous material. Given the high attenuation of acoustic waves in air-saturated porous media, multiple reflections are negligible. For reflections at the interfaces $x = 0$ and $x = L$, the expressions of the operators of reflection and transmission are simplified (Ref. [4]) as follows:

$$\tilde{R}(t) = \frac{\sqrt{\alpha_\infty} - \phi}{\sqrt{\alpha_\infty} + \phi}\delta(t) - \frac{4\phi\sqrt{\alpha_\infty}(\sqrt{\alpha_\infty} - \phi)}{(\sqrt{\alpha_\infty} + \phi)^3} G\left(t, \frac{2L}{c}\right), \tag{33}$$

$$\tilde{T}(t) = \frac{4\phi\sqrt{\alpha_\infty}}{(\phi + \sqrt{\alpha_\infty})^2} G\left(t + \frac{L}{c}, \frac{L}{c}\right). \tag{34}$$

The first term on the second member of the equation (33):
$((\sqrt{\alpha_\infty}-\phi)/(\sqrt{\alpha_\infty}+\phi))\,\delta(t)$ is equivalent to the instantaneous reflection response of the porous material. This term corresponds to the wave reflected by the first interface x = 0 . It depends only on the porosity and tortuosity of the material. The reflected wave to the first interface has the advantage not to be dispersive, but simply attenuated. This shows that it is possible to measure the porosity and tortuosity of the porous material by measuring just the first reflected wave.

The second term of equation (33): $-\frac{4\phi\sqrt{\alpha_\infty}(\sqrt{\alpha_\infty}-\phi)}{(\sqrt{\alpha_\infty}+\phi)^3}G\left(t,\frac{2L}{c}\right)$ corresponds to the reflection by the second interface $x = L$. This term depends on the Green function of the medium that describes the propagation and scattering of the acoustic wave having made a round trip in the slab of porous material. Green's function depends on the tortuosity, and viscous and thermal characteristic lengths Λ and Λ' material, but does not depend on the porosity. Experimentally, this second contribution to the debate can not be measured for low-resistive materials, because the acoustic signal is very attenuated.

Let us study the sensitivity [20] of porosity on the transmission operator $\tilde{T}(t)$. Taking the derivative of $\tilde{T}(t)$ versus the porosity ϕ, we obtain:

$$\frac{\partial\tilde{T}}{\partial\phi}=\frac{4\sqrt{\alpha_\infty}(\sqrt{\alpha_\infty}-\phi)}{(\sqrt{\alpha_\infty}+\phi)^3}G\left(t+\frac{L}{c},\frac{L}{c}\right),$$

when $\phi\longrightarrow\sqrt{\alpha_\infty}$, the derivative $\frac{\partial\tilde{T}}{\partial\phi}\longrightarrow 0$. This shows that when the porous medium tends to a free fluid, or for weakly resistive porous material with low values of porosity and tortuosity (near 1), the sensitivity of the porosity of the transmitted wave tends to zero. More generally, for a wide range of air saturated porous materials, the term $\frac{\partial\tilde{T}}{\partial\phi}$ is very small. Finally, we conclude that the operator of transmission depends on all parameters, but the low sensitivity of the porosity, makes impossible the determination of this parameter from transmitted data.

2.9. Numerical simulations

Let us consider a sample of air saturated porous M1 having the following physical properties: thickness 0.8 cm, tortuosity $\alpha_\infty = 1.5$, viscous characteristic length $\Lambda = 25\ \mu$ m, thermal characteristic length $\Lambda = 75\mu$ m, specific resistance to fluid flow σ = 200,000 Nm $^{-4}$ s, porosity $\phi = 0.82$ and thermal permeability $k_0' = 2.77\,10^{-10}$ m ^{2}. A simulated transmitted signal was calculated from the equation (31). The input signal is given in figure 3 and its spectrum in Figure 4. Figure 5 shows a comparison between two signals, the first (solid line) corresponds to the real part of the solution (28) of Pride-Lafarge model when $\wp = \wp' = 0.7$ and the second (dotted) corresponds to the solution (22) model of Johnson-Allard ($\wp = \wp' = 1$). We choose the same values for $\wp$ and $\wp'$ to simplify the study. This specific value of 0.7 is only valid for porous materials with circular pores. In the general case, the values of $\wp$ and $\wp'$ may be different from 0.7. Note that it is possible to have positive values of Δ (Eq. 18) for other values of $\wp$ and $\wp'$. From Figure 5, we notice a significant change in the wave amplitude. By increasing $\wp$ and $\wp'$ from 0.7 to 1, the wave amplitude increases by 65% of its original value. This result can be predicted by the fact that when the values of $\wp$ and $\wp'$ increases, the coefficient C decreases, and hence the wave amplitude decreases due to interactions; inertial, viscous and thermal between fluid and structure. This phenomenon is much more important for resistive porous materials. Figure 6 shows the same comparison as Figure 5 for another

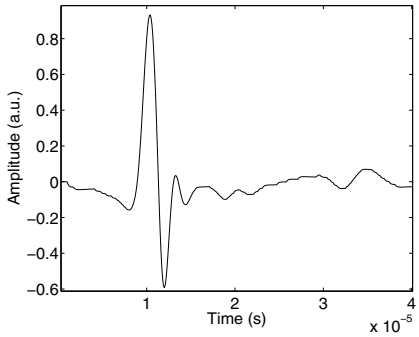

Figure 3. Incident signal

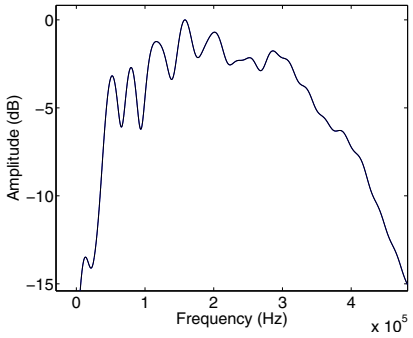

Figure 4. Spectrum of the incident signal

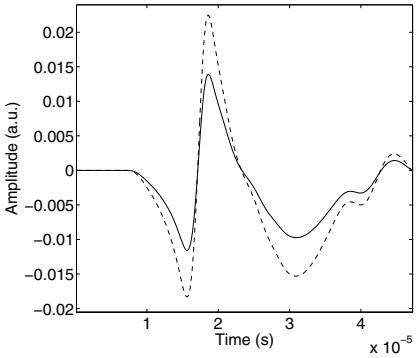

Figure 5. Comparison between simulated transmitted signal corresponding to the real part of the solution of Pride-Lafarge (Eq. 28) for $\wp = \wp' = 0.7$ (solid line) and simulated signal corresponding to the solution of Johnson-Allard (Eq. 22) for $\wp = \wp' = 1$ (dotted line) for the sample M1.

sample M2 less resistive, having the following parameters: thickness 0.8 cm, tortuosity $\alpha_\infty =$ 1.05, viscous characteristic length $\Lambda = 300$ μ m, thermal characteristic length Λ' 900 = μ m,

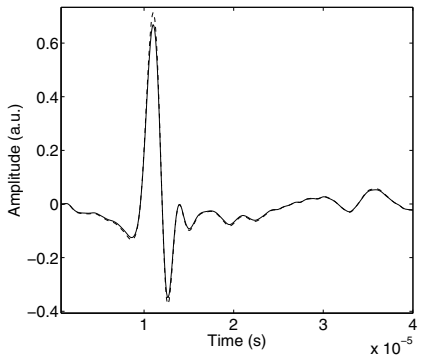

Figure 6. Comparison between simulated transmitted signal corresponding to the real part of the solution of Pride-Lafarge (Eq. 28) for $\wp = \wp' = 0.7$ (solid line), and the transmitted signal corresponding to the simulated Allard-Johnson solution (Eq. 22) for $\wp = \wp' = 1$ (dotted line) for the sample M2.

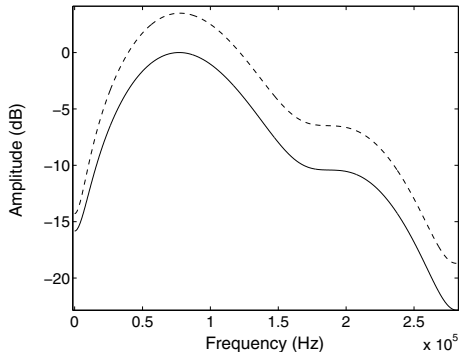

Figure 7. Spectrum of the transmitted signal simulated for $\wp = \wp' = 0.7$ Eq. (28) (solid line) and simulated transmitted signal spectrum for $\wp = \wp' = 1$ (Eq. 22) (poitillés).

specific resistance to the passage of fluid σ $=$20000$Nm-4$ s, porosity $\phi = 0.96$ and thermal permeability $k_0' = 2.77\,10^{-9}$ m ^{2}. In Figure 6, the influence of the parameters $\wp$ and $\wp'$ on the attenuation is smaller than that in Figure 5. We can conclude that the parameters $\wp$ and $\wp'$ play an important role in the acoustic attenuation, especially for resistive media.

It is possible to see from Figures 5 and 6, when the values of $\wp$ and $\wp'$ change from 0.7 to 1, the waveform changes only at the amplitude of the wave, but it is not dispersed. Figure 7 shows the spectra of two simulated signals given in Figure 5. From the spectra of two simulated signals, we can see they have the same bandwidth, which means that there is no dispersion. This last result shows that $\wp$ and $\wp'$ play an important role in attenuation the acoustic wave but not on its dispersion. Figure 8 shows the imaginary part of the solution (28) for $\wp = \wp' = 0.7$ (sample M1). The amplitude of the imaginary part of the solution is very small compared to the real part (figure 5), this is why only the real part of the solution corresponding to the physical solution is taken into account when a comparison with the experiment is performed. It is possible to write the Green function given by equation (29) as $G = G1 + iG2 =\mid G \mid e^{i\theta}$,

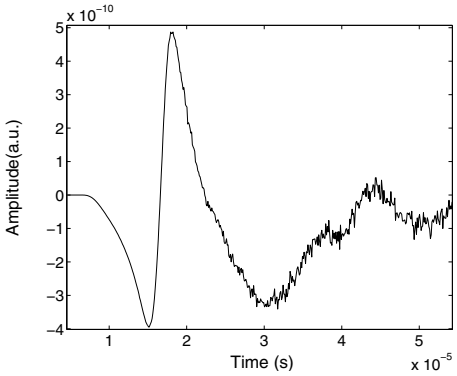

Figure 8. Simulated transmitted signal corresponding to the imaginary part of the solution (28) model of Pride-Lafarge.

$\tan\theta = G_2/G_1 \ll 1$. This leads to the conclusion that all components of the signal have the same phase (very small θ, which is therefore a physical factor not essential.

2.10. Transmitted wave

The expression (34) shows that the transmitted wave depends on the porosity ϕ, and parameters describing the high frequency acoustic propagation in the material (tortuosity α_∞ and viscous and thermal characteristic lengths Λ and Λ'). The study of the sensitivity of the porosity (in the previous paragraph) showed that the effect of propagation described by the Green's function altogether mask the effect of interfaces: recall that the Green function G is independent of porosity and the effect of the interface appears through the term $\frac{4\phi\sqrt{\alpha_\infty}}{(\phi+\sqrt{\alpha_\infty})^2}$ in the expression of the transmission operator (34). The low sensitivity of the porosity in transmission makes its determination impossible. Solving the inverse problem, using the transmitted waves allowed the determination of the tortuosity and viscous and thermal characteristic lengths. Note that the ratio of two lengths was set at 3 [20–23]. Currently the only method for the separate determination of the two lengths is based on the saturation of the porous by two different fluids [24]. The two characteristic lengths are acting the same way on the dispersion and attenuation of the transmitted signal. So it is mathematically impossible to trace two unknowns giving the same physical effect on the waveform. We limit ourselves in our work to set an arbitrary ratio between the two lengths. The tortuosity acts on the speed of the wavefront (delay of the transmitted signal with respect to the incident signal) and the attenuation of the amplitude of the waveform. While the characteristic lengths affect the dispersion and attenuation of the signal. A basic inverse problem associated with a slab of porous material may be stated as follows: from the measurements of the transmitted signals outside the slab, find the values of the parameters of the medium. As shown in the previous section, the solution of the direct problem is the system of two operators expressed as functions on α_∞, Λ and Λ'. The inversion algorithm for finding the values of the parameters of the slab is based on a fitting procedure: find the values of the parameters α_∞, Λ and Λ' such that the transmitted and reflected signal describes the scattering problem in the best possible way (e.g., in the least-squares sense). Experiments were performed in air using a pairs of broadband Ultran transducers NCG200-D13 with a central frequency of 195 kHz and

a bandwith of 6 dB extending from 140 kHz to 250 kHz. Pulses of 400 V are provided by a 5058PR Panametrics pulser/receiver. The received signals are filtered above 1 MHz to avoid high frequency noise. Electronic interference is eliminated by 1000 acquisition averages. The experimental setup is shown in Fig. 9. Consider a sample of plastic foam, of thicknesses

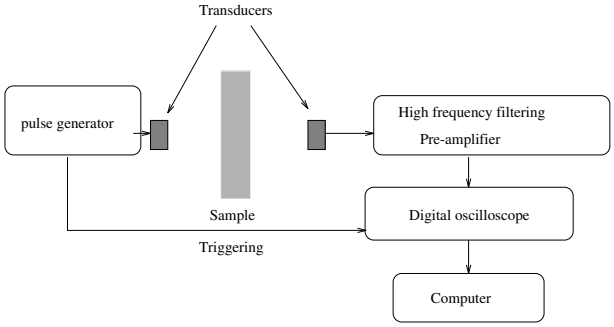

Figure 9. Experimental set-up of the ultrasonic measurements in transmitted mode.

$0.7 \pm 0.01cm$. The measured signal generated by the transducer (measured without the sample) is given in Fig. 10 as a dashed line. The measured transmitted signal (obtained with the sample inserted) is given in the same figure (Fig. 11) as a solid line. By solving the inverse problem using the experimental transmitted data, we find the following optimized values: $\alpha_\infty = 1.26$ and $\Lambda = 66\mu m$. In Figs. 11, we compare the experimental transmitted signal and simulated transmitted signal for the optimized values of tortuosity and viscous characteristic length. The difference between experiment and theory is slight, which leads us to conclude that the physical parameters are well-identified.

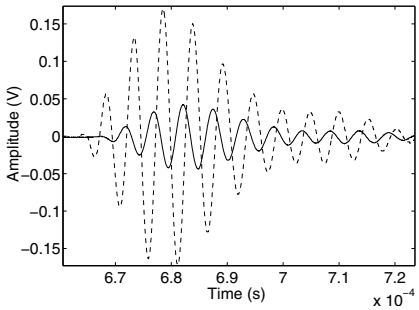

Figure 10. Experimental incident signal (dashed line) and transmitted signal (solid line) using the pair of transducers Ultran NCG200-D13 (140 kHz - 250 kHz).

2.11. Determination of transport parameters in air-saturated porous materials via reflected ultrasonic waves

A method for measuring transport parameters in porous materials simultaneously, using measurements of waves reflected at the first and second interface, has been proposed

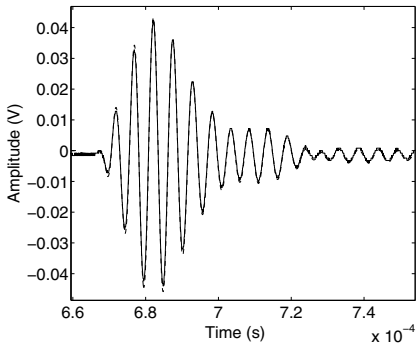

Figure 11. Comparison between experimental transmitted signal (solid line) and simulated transmitted signal (dashed line).

[25]. This method is based on a temporal model of direct and inverse scattering problems affecting the propagation of transient ultrasonic waves in a homogeneous isotropic slab of porous material with a rigid frame. Generally, porosity and tortuosity can be evaluated simultaneously by the wave reflected at the first interface at oblique incidence [26–29] but this is not possible at normal incidence [4, 30]. Viscous and thermal characteristic lengths can be estimated only by transmitted waves. Porosity cannot be determined from transmitted waves because of its weak sensitivity in this mode [4]. The advantage of the proposed method is that all the parameters can be determined at normal incidence (the ratio between viscous and thermal lengths is fixed as in classical methods [21–24] based on transmission measurement). The main principle of this method is the experimental detection of reflected contributions from the first and the second interface of the medium. The properties of these two contributions are used to estimate the four acoustical parameters needed for ultrasonic propagation in porous material with a rigid frame, by solving the inverse problem. Studying the sensitivity of each reflected wave parameter demonstrates the importance of each contribution) first and second interface! for the inversion. Numerical and experimental validation for weak resistive air-saturated industrial plastic foams is given to validate this method.

2.12. Reflected and transmitted waves

This section concerns the ultrasonic characterization of air-saturated porous materials by solving the inverse problem using experimental data. It is generally easy to solve the inverse problem via transmitted waves, obtaining optimized values of tortuosity, viscous and thermal characteristic lengths, but this is not the case for the porosity because of its weak sensitivity in the transmitted mode. The reflection mode is an alternative to the transmission mode, in that it gives a good estimation of porosity and tortuosity by processing the data relative to measurements of the wave reflected by the first interface. The viscous and thermal characteristic lengths cannot be determined via the first interface reflection. The wave reflected by the second interface can be experimentally detected only for the weakly resistive porous materials. In this case, the characteristic lengths can be estimated. But for common air-saturated porous materials, the second reflection is very damped and its experimental detection is difficult. We solve the inverse problem [31] numerically by the least-squares method, using both reflected and transmitted experimental data. We determine

simultaneously all the physical parameters intervening in the propagation. The minimization between experiment and theory is made in the time domain. The inverse problem is well posed, and its solution is unique. As with the classic ultrasonic approach for characterizing porous material saturated with one gas, the characteristic lengths are estimated by assuming a given ratio between them. Tests are performed using industrial plastic foams. Experimental and numerical results, and prospects are discussed [31].

2.13. Ultrasonic characterization of air-saturated double-layered porous media

This section concerns a time-domain model of transient wave propagation in double-layered porous materials [32]. An analytical derivation of reflection and transmission scattering operators is given in the time domain. These scattering kernels are the medium's responses to an incident acoustic pulse. The expressions obtained take into account the multiple reflections occurring at the interfaces of the double-layered material. The double-layered porous media consist of two slabs of homogeneous isotropic porous materials with a rigid frame. Each porous slab is described by a temporal equivalent fluid model, in which the acoustic wave propagates only in the fluid saturating the material. In this model, the inertial effects are described by the tortuosity; the viscous and thermal losses of the medium are described by two susceptibility kernels which depend on the viscous and thermal characteristic lengths. the inverse problem is solved using experimental reflected signals at normal incidence. The sensitivity of porosity, tortuosity, and viscous characteristic length of each layer is studied showing their effect on the reflected interface waveforms. The inverse problem is solved numerically by the least-squares method. Five parameters are inverted: porosity and tortuosity of the two layers and the viscous characteristic length of the first layer. The minimization of the discrepancy between experimental and theoretical data is made in the time domain. The inverse problem is shown to be well posed and its solution to be unique. Experimental results for waves reflected by the interfaces of the double-layered porous material are given and compared with theoretical predictions [32].

2.14. Acoustic characterization of porous materials at low frequency range

In this frequency range, the viscous forces are important throughout the fluid, the cycle of compression/expansion in the porous medium is slow enough to allow heat exchange between fluid and structure. At the same time, the temperature of the structure is practically unchanged by the passage of the sound wave due to the large value of its specific heat conducting relation to that of the fluid: the structure acts as a thermostat. In this case the isothermal compression is directly applicable. This range corresponds to frequencies where the viscous skin depth $\delta = (2\eta/\omega\rho_f)^{1/2}$ is larger than the pore radius.

An acoustic method [33–37] using transmitted and reflected waves is proposed for measuring static viscous permeability k_0, flow resistivity σ, static thermal permeability k_0' and the inertial factor α_0 (low frequency tortuosity), of porous materials having a rigid frame at low frequencies. Flow resistivity of porous material is defined as the ratio between the pressure difference across a sample and the velocity of flow of air through that sample per unit cube. The static thermal permeability of porous material is a geometrical parameter equal to the inverse trapping constant of the solid frame. The inertial factor describes the fluid structure interactions in the low frequency range (1-3 kHz). These parameters are determined from the

solution of the inverse problem. The propagation equation is given (along the $x-$axis) by:

$$\frac{\partial^2 p(x,t)}{\partial x^2} - \frac{1}{c^2}\frac{\partial^2 p(x,t)}{\partial t^2} - A\frac{\partial p(x,t)}{\partial t} + B\frac{\partial^3 p(x,t)}{\partial t^3} = 0, \tag{35}$$

$$\frac{1}{c^2} = \frac{\rho_f}{K_a}\left(\alpha_0\gamma - \frac{(\gamma-1)P_r k_0'}{k_0}\right), \quad A = \frac{\eta\phi}{\rho_f k_0},$$

$$B = -\frac{\alpha_0(\gamma-1)k_0' P_r \rho_f^2}{K_a\eta\phi} + \frac{\alpha_0'(\gamma-1){k_0'}^2 {P_r}^2 {\rho_f}^2}{\eta\phi k_0 K_a} - \frac{\gamma\alpha_\infty\rho_f^2\Lambda^2\left(\frac{\alpha_0}{\alpha_\infty}-1\right)^3}{4\eta K_a}$$

The solution of this equation gives the Green function [34] of the porous material:

$$G(x,t) = \frac{1}{\sqrt{\pi}}\frac{x}{c}\sqrt{b'}\left[\frac{\sqrt{\Delta}}{4\,b'}\frac{1}{t^{3/2}}\exp\left(-\frac{x^2\Delta}{16c^2\,b'\,t}\right) - \frac{2}{\pi\sqrt{\pi}}\int_{\frac{x}{c}\sqrt{b'}}^{\infty}\frac{F(\zeta,t)}{\sqrt{\zeta^2-\frac{x^2}{c^2}b'}}d\zeta\right],$$

$$F(\zeta,t) = \int_0^\infty \exp(-s\,t)\sqrt{s}(s+1/2b')\aleph(\zeta,s)ds,$$

$$\aleph(\zeta,s) = \int_{-1}^{1}\cos\left[\frac{\sqrt{\Delta}}{2b'}\zeta\sqrt{s} - y\sqrt{s}(s+1/2b')\sqrt{\zeta^2-\frac{x^2}{c^2}b'}\right]\frac{y\,d\,y}{\sqrt{1-y^2}},$$

$$b' = Bc^2, c' = Ac^2, \Delta = 1+4b'c'.$$

The incident $p^i(t)$ and transmitted $p^t(t)$ fields are related in time domain by the transmission scattering operator 31. Its expression is given by the relation given in Ref. [34]:

$$\tilde{T}(t) = \int_0^t D(\tau)G(t-\tau+L/c, L/c)d\tau, - * \tag{36}$$

$$D(t) = \frac{2}{\varpi\sqrt{\pi}}\frac{1}{t^{3/2}}\int_0^\infty\left(\frac{u^2}{2t}-1\right)u\exp\left(-\frac{u}{\varpi}-\frac{u^2}{4t}\right)du, \qquad \varpi = \sqrt{\frac{\rho_f k_0\gamma\pi}{\eta}}.$$

In the very low frequency range, the propagation equation 35 is reduced to a diffusive equation

$$\frac{\partial^2 p(x,t)}{\partial x^2} - d\frac{\partial p(x,t)}{\partial t} = 0, \tag{37}$$

where $d = \frac{\sigma\phi\gamma}{K_a}$ the diffusion constant. The solution of this diffusive equation gives the Green function of the porous material [33, 35, 36]:

$$G(x,t) = \frac{x\sqrt{d}}{2\sqrt{\pi}}\frac{1}{t^{3/2}}\exp\left(-\frac{x^2\,d}{4t}\right). \tag{38}$$

The transmission scattering operator is $\tilde{T}(t) = D(t) * G(L,t)$, where * denotes the time convolution operation. The operator $D(t)$ is given by

$$D(t) = -\frac{8}{B^2}\left(1+\frac{t}{B^2}\right)\exp\left(\frac{t}{B^2}\right)\mathrm{Erfc}\left(\frac{\sqrt{t}}{B}\right) + \frac{4}{B\sqrt{\pi t}}\left(2\frac{t}{B^2}+1\right), \qquad B = \frac{1}{\eta}\sqrt{\phi^3\gamma\sigma^3\rho_f},$$

where Erfc is the complementary error function and ρ_f is the fluid density.

The inverse problem is to find the parameters k' and α_0 [37] which minimize numerically the discrepancy function $U(k', \alpha_0) = \sum_{i=1}^{i=N} (p^t_{exp}(x, t_i) - p^t(x, t_i))^2$, wherein $p^t_{exp}(x, t_i)_{i=1,2,...n}$ is the discrete set of values of the experimental transmitted signal and $p^t(x, t_i)_{i=1,2,...n}$ the discrete set of values of the simulated transmitted signal predicted from Eq. (31). The inverse problem is solved numerically by the least-square method. For its iterative solution, we used the simplex search method (Nedler Mead) [38] which does not require numerical or analytic gradients. Experiments are performed in a guide [33–37] (pipe), having a diameter of 5 cm. The experimental set up is given in Fig. 12. For measuring the static thermal permeability and the inertial factor, a pipe of 3 m long, since the frequencies used in the experiment are between 1kHz and 4 kHz. However, for measuring the viscous permeability (and flow resistivity) [33, 35, 36], a pipe of 50 m long must be used (50Hz-1kHz) to avoid the reflections at its end. In this case, it is not important to keep the pipe straight, it can be rolled in order to save space without perturbations on experimental signals (the cut-off frequency of the tube $f_c \sim$ 4kHz). A sound source Driver unit "Brand" constituted by loudspeaker Realistic 40-9000 is used. Bursts are provided by synthesized function generator Standford Research Systems model DS345-30MHz. The signals are amplified and filtered using model SR 650-Dual channel filter, Standford Research Systems. The signals (incident and transmitted) are measured using the same microphone (Bruel&Kjaer, 4190) in the same position in the tube. The incident signal is measured without porous sample, however, the transmitted signal is measured with the porous sample. Consider a cylindrical sample of plastic foam M of diameter 5 cm, porosity $\phi = 0.85$ and thickness 4.15 cm. The viscous permeability k_0 of the porous sample is measured by solving the inverse problem in time domain at viscous domain (very low frequency range)[33, 35, 36]. The obtained value of k_0 is $(0.44 \pm 0.02) \times 10^{-9}\ m^2$. The static thermal permeability is measured using classic Kundt tube (continuous frequency) [39] (continuous frequency) obtaining the value of $k'_0 = (1.54 \pm 0.05) \times 10^{-9}$, with a ratio of 3.5 between k'_0 and k_0. The tortuosity α_∞ and the viscous characteristic length Λ are measured in the high frequency range [4] obtaining the values: $\alpha_\infty = 1.2$ and $\Lambda = 65\mu m$. The value of the thermal tortuosity α'_0 is approximated by the relation $\alpha'_0 \simeq \alpha_0/\alpha_\infty$. Fig. 13 shows the experimental incident signal (solid line) generated by the loudspeaker in the frequency bandwidth (2.5 - 3.5) kHz, and the experimental transmitted signal (dashed line). After solving the inverse problem numerically for the thermal permeability k'_0 and the inertial factor α_0 , we find the following optimized values: $k'_0 = (1.06 \pm 0.2) \times 10^{-9} m^2$ and $\alpha_0 = 2.15 \pm 0.15$. We present in Fig. 14 the variation of the minimization function U with the thermal permeability k'_0 and tortuosity α_0. The obtained ratio of 2.4 between the inverted k'_0 and k_0 is in adequacy with the ratio given in literature [9, 39], which is found generally to be between 2 and 4 for plastic foams. In Fig. 15, we show a comparison between an experimental transmitted signal and simulated transmitted signal for the optimized values of thermal permeability and tortuosity. The difference between the two curves is slight, which leads us to conclude that the optimized values of the thermal permeability and inertial factor are correct. This study has been carried out, in the frequency bandwidths (1.5 - 2.5) kHz and has also given good results.

3. Modified Biot theory

When the structure of a porous material is not rigid, the equivalent fluid model, on which the previous sections are based, no longer applies because the waves propagate in both the

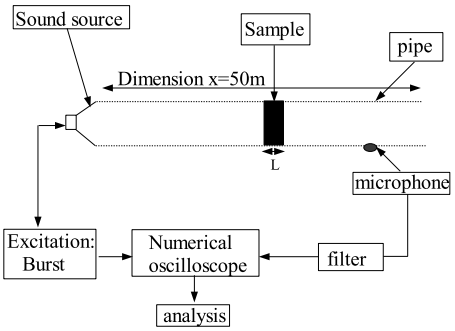

Figure 12. Experimental setup of acoustic measurements.

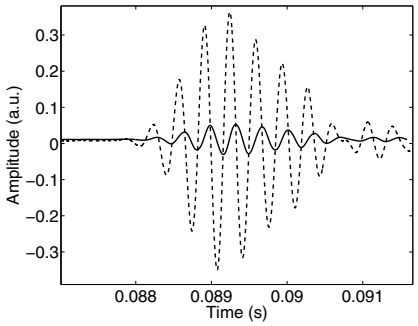

Figure 13. Experimental incident signal (solid line) and experimental transmitted signal (dashed line).

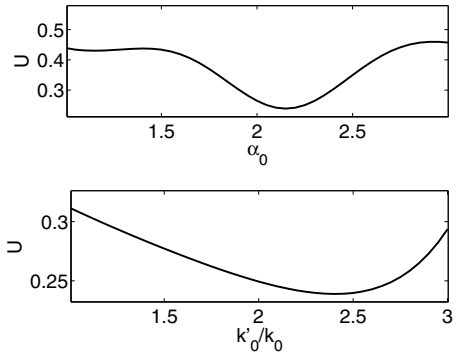

Figure 14. Minima of the inverse problem.

skeleton and the saturating fluid. The fluid-structure interactions then play an essential role in the propagation. The study of theses effects has been largely developed by Biot [40, 41] for applications in the domain of oil exploration since 1950. This semi-phenomenological theory provides a rigorous description of the propagation of acoustical waves in porous

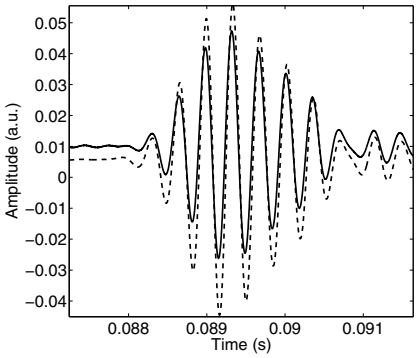

Figure 15. Comparison between the experimental transmitted signal (solid line) and the simulated transmitted signals (dashed line) using the reconstructed values of k_0' and α_0.

media saturated by a compressible viscous fluid. Such diphasic materials are supposed to be elastic and homogeneous. Biot's theory was initially introduced for petroleum prospecting and research. Due to its very general and rather fundamental character, it has been applied in various fields of acoustics such as geophysics, underwater acoustics, seismology, ultrasonic characterization of bones, etc. Cancelous bone is a porous material consisting of a matrix of solid trabeculae filled with soft bone marrow. The interaction between ultrasound and bone is highly complex. Modeling ultrasonic propagation through trabecular tissue has been considered using porous media theories, such as Biot's theory. This theory derives the equations of motion for each phase (i.e. the solid frame and the fluid) based on energy considerations which include the inertial, potential and viscous coupling between the two phases. For an isotropic porous medium, three different bulk modes are predicted, i.e. two compression waves and one shear wave. One compressional wave, the so-called wave of the first type or fast longitudinal wave, and the transverse wave are similar to the two bulk waves observed in an anisotropic linear elastic solid. The other longitudinal wave, called a wave of the second kind, or slow wave, is a highly damped and very dispersive mode. It is diffusive at low frequencies and propagative at high frequencies. In this section, the direct and inverse scattering problems for the ultrasonic propagation in porous material having an elastic frame are solved [42–46]. An experimental application on human cancelous bone is discussed [42, 43].

3.1. Model

The equations of motion of the frame and fluid are given by the Euler equations applied to the Lagrangian density. Here $\overrightarrow{u}$ and $\overrightarrow{U}$ are the displacements of the solid and fluid phases. The equations of motion are:

$$\begin{aligned}
\widetilde{\rho}_{11}(t) * \frac{\partial^2 \overrightarrow{u}}{\partial t^2} + \widetilde{\rho}_{12}(t) * \frac{\partial^2 \overrightarrow{U}}{\partial t^2} &= P\overrightarrow{\nabla}.(\overrightarrow{\nabla}.\overrightarrow{u}) + Q\overrightarrow{\nabla}(\overrightarrow{\nabla}.\overrightarrow{U}) - N\overrightarrow{\nabla} \wedge (\overrightarrow{\nabla} \wedge \overrightarrow{u}),\\
\widetilde{\rho}_{12}(t) * \frac{\partial^2 \overrightarrow{u}}{\partial t^2} + \widetilde{\rho}_{22}(t) * \frac{\partial^2 \overrightarrow{U}}{\partial t^2} &= Q\overrightarrow{\nabla}(\overrightarrow{\nabla}.\overrightarrow{u}) + R\overrightarrow{\nabla}(\overrightarrow{\nabla}.\overrightarrow{U}).
\end{aligned} \tag{39}$$

wherein P, Q and R are generalized elastic constants which are related, via gedanken experiments, to other, measurable quantities, namely ϕ (porosity), K_f (bulk modulus of the pore fluid), K_s (bulk modulus of the elastic solid) and K_b (bulk modulus of the porous skeletal frame). N is the shear modulus of the composite as well as that of the skeletal frame. The equations which explicitly relate P, Q, and R to ϕ, K_f, K_s, K_b, and N are given by

$$P=\frac{(1-\phi)(1-\phi-\frac{K_b}{K_s})K_s+\phi\frac{K_s}{K_f}K_b}{1-\phi-\frac{K_b}{K_s}+\phi\frac{K_s}{K_f}}+\frac{4}{3}N,\quad Q=\frac{(1-\phi-\frac{K_b}{K_s})\phi K_s}{1-\phi-\frac{K_b}{K_s}+\phi\frac{K_s}{K_f}},\quad R=\frac{\phi^2K_s}{1-\phi-\frac{K_b}{K_s}+\phi\frac{K_s}{K_f}}.$$

The Young modulus and the Poisson ratio of the solid E_s, ν_s and of the skeletal frame E_b, ν_b depend on the generalized elastic constant P, Q and R via the relations:

$$K_s=\frac{E_s}{3(1-2\nu_s)},\qquad K_b=\frac{E_b}{3(1-2\nu_b)},\qquad N=\frac{E_b}{2(1+\nu_b)}. \tag{40}$$

The temporal operators $\widetilde{\rho}_{11}(t)$, $\widetilde{\rho}_{12}(t)$ et $\widetilde{\rho}_{22}(t)$ are the operators of mass coupling between fluid and structure and are given in the high frequency range by [47]:

$$\widetilde{\rho}_{11}(t)=\rho_{11}+\frac{2\phi\alpha_\infty}{\Lambda}\left(\frac{\rho_f\eta}{\pi t}\right)^{1/2},\quad \widetilde{\rho}_{12}(t)=\rho_{12}-\frac{2\phi\alpha_\infty}{\Lambda}\left(\frac{\rho_f\eta}{\pi t}\right)^{1/2},$$
$$\widetilde{\rho}_{22}(t)=\rho_{22}+\frac{2\phi\alpha_\infty}{\Lambda}\left(\frac{\rho_f\eta}{\pi t}\right)^{1/2}.$$

Biot coefficients ρ_{mn}, are the "mass factors" and are connected to the densities of solid (ρ_s) and fluid (ρ_f) by $\rho_{11}+\rho_{12}=(1-\phi)\rho_s$ and $\rho_{12}+\rho_{22}=\phi\rho_f$, $\rho_{12}=-\phi\rho_f(\alpha_\infty-1)$.

3.1.1. Longitudinal waves

As in the case of an elastic solid, the wave equations of dilatational and rotational waves can be obtained using scalar and vector displacement potentials, respectively. Two scalar potentials for the frame and the fluid Φ_s and Φ_f

$$\overrightarrow{u}=\overrightarrow{\nabla}\Phi_s,\qquad \overrightarrow{U}=\overrightarrow{\nabla}\Phi_f.$$

In this case the equations 39 become for a propagation along the x axis:

$$\begin{pmatrix}\rho_{11}&\rho_{12}\\ \rho_{12}&\rho_{22}\end{pmatrix}\frac{\partial^2}{\partial t^2}\begin{pmatrix}\Phi_s\\ \Phi_f\end{pmatrix}+\frac{2\phi\rho_f\alpha_\infty}{\Lambda}\sqrt{\frac{\eta}{\rho_f}}\begin{pmatrix}1&-1\\ -1&1\end{pmatrix}\frac{\partial^{3/2}}{\partial t^{3/2}}\begin{pmatrix}\Phi_s\\ \Phi_f\end{pmatrix}=\begin{pmatrix}P&Q\\ Q&R\end{pmatrix}\frac{\partial^2}{\partial x^2}\begin{pmatrix}\Phi_s\\ \Phi_f\end{pmatrix}, \tag{41}$$

The result of solving this system of equations is the existence of two distinct longitudinal modes called slow mode and fast mode. The system (41) can be expressed on the basis of slow and fast waves Φ_1 and Φ_2 respectively by:

$$\frac{\partial^2}{\partial x^2}\begin{pmatrix}\Phi_1\\ \Phi_2\end{pmatrix}=\begin{pmatrix}\widetilde{\lambda}_1(t)&0\\ 0&\widetilde{\lambda}_2(t)\end{pmatrix}\begin{pmatrix}\Phi_1\\ \Phi_2\end{pmatrix},$$

where $\widetilde{\lambda}_1(t)$ and $\widetilde{\lambda}_2(t)$ are operators of time corresponding to the eigenvalues of the system (41). Their expressions are given by:

$$\widetilde{\lambda}_1(t) = \frac{1}{2}\left(\tau_1 - \sqrt{\tau_1^2 - 4\tau_3}\right)\frac{\partial^2}{\partial t^2} + \frac{1}{2}\left(\tau_2 - \frac{\tau_1\tau_2 - 2\tau_4}{\sqrt{\tau_1^2 - 4\tau_3}}\right)\frac{\partial^{3/2}}{\partial t^{3/2}} - \frac{1}{4}\left(\frac{\tau_2^2}{\sqrt{\tau_1^2 - 4\tau_3}} - \frac{(\tau_1\tau_2 - 2\tau_4)^2}{2(\tau_1^2 - 4\tau_3)^{3/2}}\right)\frac{\partial}{\partial t},$$

$$\widetilde{\lambda}_2(t) = \frac{1}{2}\left(\tau_1 + \sqrt{\tau_1^2 - 4\tau_3}\right)\frac{\partial^2}{\partial t^2} + \frac{1}{2}\left(\tau_2 + \frac{\tau_1\tau_2 - 2\tau_4}{\sqrt{\tau_1^2 - 4\tau_3}}\right)\frac{\partial^{3/2}}{\partial t^{3/2}} + \frac{1}{4}\left(\frac{\tau_2^2}{\sqrt{\tau_1^2 - 4\tau_3}} - \frac{(\tau_1\tau_2 - 2\tau_4)^2}{2(\tau_1^2 - 4\tau_3)^{3/2}}\right)\frac{\partial}{\partial t}$$

with:

$\tau_1 = R'\rho_{11} + P'\rho_{22} - 2Q'\rho_{12}$, $\tau_2 = A\left(P' + R' + 2Q'\right)$, $\tau_3 = \left(P'R' - Q'^2\right)\left(\rho_{11}\rho_{22} - \rho_{12}^2\right)$,

and $\tau_4 = A\left(P'R' - Q'^2\right)\left(\rho_{11} + \rho_{22} - 2\rho_{12}\right)$.

Coefficients R', P' and Q' are given by: $R' = \frac{R}{PR - Q^2}$, $Q' = \frac{Q}{PR - Q^2}$, and $P' = \frac{P}{PR - Q^2}$. The system of equations (41) shows that the slow and fast waves obey the same propagation equation developed in the framework of the equivalent fluid model (equation 13). The eigenvectors $(1, \widetilde{\Im}_1(t))$ and $(1, \widetilde{\Im}_2(t))$ associated with the eigenvalues $\widetilde{\lambda}_1(t)$ et $\widetilde{\lambda}_2(t)$ link the potential solid and fluid Φ_s and Φ_f, respectively to slow and fast waves Φ_1 and Φ_2 by the following relations:

$$\begin{pmatrix} \Phi_s \\ \Phi_f \end{pmatrix} = \begin{pmatrix} 1 & 1 \\ \widetilde{\Im}_1(t) & \widetilde{\Im}_2(t) \end{pmatrix}\begin{pmatrix} \Phi_1 \\ \Phi_2 \end{pmatrix}, \tag{42}$$

the analytical expressions of temporal operators $\widetilde{\Im}_1(t)$ and $\widetilde{\Im}_2(t)$ are given by:

$$\widetilde{\Im}_1(t) = \frac{\tau_1 - 2\tau_5 - \sqrt{\tau_1^2 - 4\tau_3}}{2\tau_7} + \frac{t^{-1/2}}{4\tau_7^2\sqrt{\pi}} \times \left[\left(\tau_2 - 2\tau_6 - \frac{\tau_1\tau_2 - 2\tau_4}{\sqrt{\tau_1^2 - 4\tau_3}}\right)2\tau_7 + \left(\tau_1 - 2\tau_5 - \sqrt{\tau_1^2 - 4\tau_3}\right)2\tau_6\right],$$

$$\widetilde{\Im}_2(t) = \frac{\tau_1 - 2\tau_5 + \sqrt{\tau_1^2 - 4\tau_3}}{2\tau_7} + \frac{t^{-1/2}}{4\tau_7^2\sqrt{\pi}} \times \left[\left(\tau_2 - 2\tau_6 + \frac{\tau_1\tau_2 - 2\tau_4}{\sqrt{\tau_1^2 - 4\tau_3}}\right)2\tau_7 + \left(\tau_1 - 2\tau_5 + \sqrt{\tau_1^2 - 4\tau_3}\right)2\tau_6\right],$$

where

$$\tau_5 = \left(R'\rho_{11} - Q'\rho_{12}\right) \quad \tau_6 = A\left(R' + Q'\right), \quad \tau_7 = \left(R'\rho_{12} - Q'\rho_{22}\right).$$

For a slab of cancellous bone occupying the region $0 \leq x \leq L$, the incident $p^i(t)$ and transmitted $p^t(t)$ fields are related in the time domain by the transmission scattering operator $\tilde{T}$ given by Eq. 31. In the frequency domain, the expression of the transmission coefficient $\mathcal{T}(\omega)$, which is the Fourier transform of $\tilde{T}$ is given by [42]

$$\mathcal{T}(\omega) = \frac{j\omega 2\rho_f c_0 F_4(\omega)}{\left(j\omega\rho_f c_0 F_4(\omega)\right)^2 - \left(j\omega F_3(\omega) - 1\right)^2}, \tag{43}$$

where

$$F_i(\omega) = \left(1 + \phi\left(\Im_i(\omega) - 1\right)\right)\sqrt{\lambda_i(\omega)}\frac{\Psi_i(\omega)}{\sinh\left(l\sqrt{\lambda_i(\omega)}\right)}\frac{2}{\Psi(\omega)}, \qquad i = 1, 2.$$

$$F_3(\omega) = \rho_f c_0\left(F_1(\omega)\cosh\left(l\sqrt{\lambda_1(\omega)}\right) + F_2(\omega)\cosh\left(l\sqrt{\lambda_2(\omega)}\right)\right), \quad F_4(\omega) = F_1(\omega) + F_2(\omega).$$

The functions $\lambda_1(\omega)$, $\lambda_2(\omega)$, $\Im_1(\omega)$ and $\Im_2(\omega)$ are the Fourier transform of $\widetilde{\lambda}_1(t)$, $\widetilde{\lambda}_2(t)$, $\widetilde{\Im}_1(t)$ and $\widetilde{\Im}_2(t)$, respectively. The coefficients $\Psi_1(\omega)$, $\Psi_2(\omega)$ and $\Psi(\omega)$ are given by

$$\Psi_1(\omega) = \phi Z_2(\omega) - (1-\phi)Z_4(\omega), \qquad \Psi_2(\omega) = (1-\phi)Z_3(\omega) - \phi Z_1(\omega),$$
$$\Psi(\omega) = 2(Z_1(\omega)Z_4(\omega) - Z_2(\omega)Z_3(\omega)),$$

and the coefficients $Z_1(\omega)$, $Z_2(\omega)$, $Z_3(\omega)$ and $Z_4(\omega)$ by

$$Z_1(\omega) = (P + Q\Im_1(\omega))\lambda_1(\omega), \quad Z_2(\omega) = (P + Q\Im_2(\omega))\lambda_2(\omega),$$
$$Z_3(\omega) = (Q + R\Im_1(\omega))\lambda_1(\omega), \quad Z_4(\omega) = (Q + R\Im_2(\omega))\lambda_2(\omega).$$

3.2. Ultrasonic characterization of human cancellous bone using the Biot theory: Inverse problem

Osteoporosis is a degenerative bone disease associated with biochemical and hormonal changes in the ageing body. These changes perturb the equilibrium between bone apposition and bone removal, resulting in a net decrease in bone mass. This leads to a modification of the structure (porosity, trabecular thickness, connectivity etc.) and, to a lesser extent, the composition (mineral density) of the bone. These changes result in a decrease of the mechanical strength of bone and in an increase of the risk of fracture. Osteoporosis mainly affects the trabecular bone (located at the hip, vertebrae or heels for instance). Early clinical detection of this pathological condition is very important to insure proper treatment. The primary method currently used for clinical bone assessment is based on x-ray absorptiometry, and measures total bone mass at a particular anatomic site. Because other factors, such as architecture, also appear to have a role in determining an individual's risk of fracture, ultrasound is an alternative to X-rays that has generated much attention. In addition to their potential for conveying the architectural aspects of bone, ultrasonic techniques also may have advantages in view of their use as a nonionising radiation and inherently lower costs,

compared with x-ray densitometric methods. Although ultrasonic methods appear promising for noninvasive bone assessment, they have not yet fulfilled their potential. Unfortunately, a poor understanding of the ultrasound interaction with bone has become one of the obstacles preventing it from being a fully developed diagnostic technique. Despite extensive research on the empirical relationship between ultrasound and the bulk properties of bone, the mechanism of how ultrasound physically interacts with bone is still unclear. Since trabecular bone is an inhomogeneous porous medium, the interaction between ultrasound and bone is a highly complex phenomenon. Modelling ultrasonic propagation through trabecular tissue has been considered using porous media theories, such as Biot's theory. As seen in the previous section, within the framework of the modified Biot theory, the propagation of ultrasonic waves in a slab of cancellous bone is conditioned by many parameters: porosity ϕ, tortuosity α_∞, viscous characteristic length Λ, fluid viscosity η, Young's modulus of the elastic solid E_s, Young's modulus of porous skeletal frame E_b, Poisson's ratio of the elastic solid ν_s, Poisson's ratio of the porous skeletal frame ν_b, the solid density ρ_s, the bulk modulus of the saturating fluid K_f and the fluid density ρ_f. It is therefore important to develop new experimental methods and efficient tools for their estimation. The basic inverse problem associated with the slab of cancellous bone may be stated as follows: from measurements of the signal transmitted outside the slab, find the values of the medium's parameters. Solving the inverse problem for all the Biot parameters using only the transmitted experimental data is difficult, if not impossible. To achieve this task, requires more experimental data for obtaining a unique solution. For this reason, in this contribution we limit the inversion to the five parameters: E_b, ν_b, ϕ, α_∞ and Λ. In our previous paper [42], we studied the sensitivity of transmitted waveforms to variations of ϕ, α_∞ and Λ. The sensitivity of E_b and ν_b has been examined in Ref. [43]

As an application of this model, some numerical simulations are compared with experimental results. Experiments are performed in water using two broadband Panametrics A 303S plane piezoelectric transducers with a central frequency of 1 MHz in water, and diameter of 1cm. 400 V Pulses are provided by a 5058PR Panametrics pulser/receiver. Electronic interference is removed by averaging 1000 acquisitions. The experimental setup is shown in Fig. 9. The parallel-faced samples were machined from femoral heads and femoral necks of human cancellous bone. The liquid in the pore space (blood and marrow) is removed from the bone sample and substituted by water. The size of the ultrasound beam is very small compared to the size of the specimens. The emitting transducer insonifies the sample at normal incidence with a short (in time domain) pulse. When the pulse hits the front surface of the sample, a part is reflected, a part is transmitted as a fast wave, and a part is transmitted as a slow wave. When any of these components, travelling at different speeds, hit the second surface, a similar effect takes place: a part is transmitted into the fluid, and a part is reflected as a fast or slow wave. The experimental transmitted waveforms are travelling through the cancellous bone in the same direction as the trabecular alignment (x direction). The fluid characteristics are: bulk modulus $K_f = 2.28$ GPa, density $\rho_f = 1000\text{Kgm}^{-3}$, viscosity $\eta = 10^{-3} Kg.m.s^{-1}$. Consider a sample of human cancellous bone M1 (femoral neck) of thickness 11.2 mm and solid density $\rho_s = 1990\text{Kgm}^{-3}$. The Young's modulus $E_s = 13GPa$ and Poisson ratio $\nu_s = 0.3$ of the solid bone are taken from the literature [48]. Figure 9 shows the experimental incident signal. The inverse problem is solved by minimizing the function $U(\phi, \alpha_\infty, \Lambda, E_b, \nu_s)$ given by:

$$U(\phi, \alpha_\infty, \Lambda, E_b, \nu_b) = \sum_{i=1}^{i=n} (p^t_{exp}(x, t_i) - p^t(x, t_i))^2,$$

wherein $p^t_{exp}(x,t_i)_{i=1,2,...n}$ is the discrete set of values of the experimental transmitted signal and $p^t(x,t_i)_{i=1,2,...n}$ the discrete set of values of the simulated transmitted signal. A large variation range is applied of each estimating parameter value in solving the inverse problem. The variation range of the parameters is ; $\alpha_\infty \in [1,2]$, $\Lambda \in [1,\ 200]\mu m$, $\phi \in [0.5, 0.99]$, $\nu \in [0.1, 0.5]$ and $E_b \in [0.5, 5]$GPa. The variations of the cost function with the physical parameters present one clear minimum corresponding to the mathematical solution of the inverse problem. This shows that the inverse problem is well posed mathematically, and that the solution is unique. The minima, corresponding to the solution of the inverse problem, are clearly observed for each parameter. After solving the inverse problem, we find the following optimized values: $\phi = 0.64$, $\alpha_\infty = 1.018$, $\Lambda = 10,44\mu m$, $\nu_b = 0.28$ and $E_b = 4.49$ GPa. Using these values, we present in Figs. 16-19 the variations in the discrepancy function U with respect to two values of the inverted parameters. To show clearly the solution of the

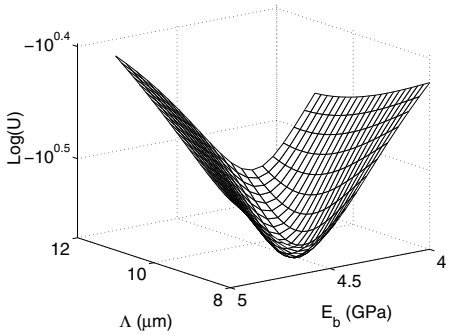

Figure 16. Variation of the minimization function U with the viscous characteristic length Λ and the Young modulus of the skeletal frame E_b.

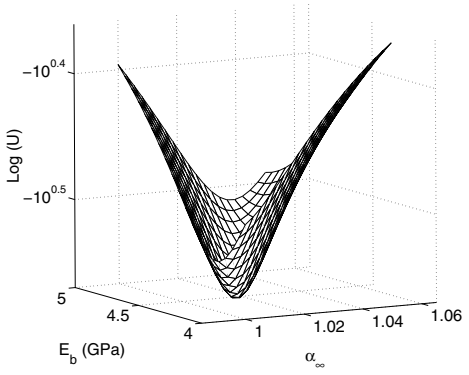

Figure 17. Variation of the minimization function U with the the Young modulus of the skeletal frame E_b and the tortuosity α_∞.

inverse problem, the variation of U in Figs. 16-19 is given only around the minima values of the inverted parameters. In Fig. 20, a comparison is made between the experimental transmitted signal and the simulated transmitted signals using the reconstructed values of

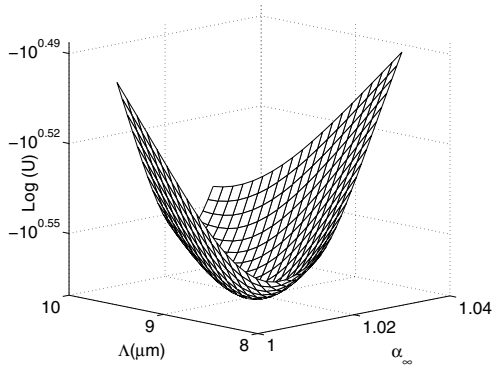

Figure 18. Variation of the minimization function U with the viscous characteristic length Λ and the tortuosity α_∞.

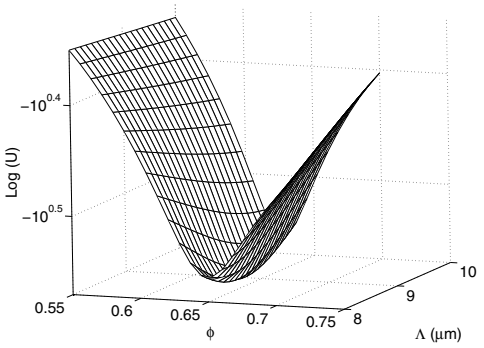

Figure 19. Variation of the minimization function U with the porosity ϕ and the viscous characteristic length Λ.

α_∞, ϕ, Λ, ν_b and E_b. The difference between the two curves is small, which leads us to conclude that the optimized values of the physical parameters are correct. The fast and slow waves predicted by the Biot theory are easily detected in the transmitted signal. The slow wave seems to be less attenuated than the fast wave. In the other applications, the slow wave is generally more-attenuated and dispersive than the fast wave. We usually observe the opposite phenomena for cancellous bone samples; this can be explained by the different orders of magnitude of the physical parameters (high porosity, low tortuosity...etc). Let us now solve the inverse problem for sample M2 (femoral neck) of thickness 12 mm. Using another sample of cancellous bone (femoral head) M2 of thickness 10.2 mm. The results after solving the inverse problem are: $\phi = 0.72$, $\alpha_\infty = 1.1$, $\Lambda = 14.97\mu m$, $\nu_b = 0.22$ and $E_b = 3.1GPa$. In Fig. 21, we compare the experimental transmitted signal to the transmitted simulated signal using reconstruct values of the physical parameters. The correlation between the two curves is excellent. The simulated transmitted signals obtained using optimized values (Figs. 20 and

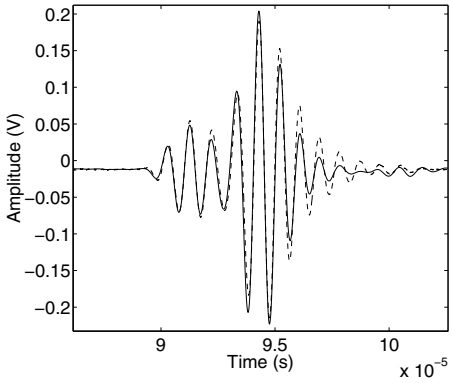

Figure 20. Comparison between the experimental transmitted signal (solid line) and the simulated transmitted signals (dashed line) using the reconstructed values of α_∞, ϕ, Λ, ν_b and E_b (sample M1).

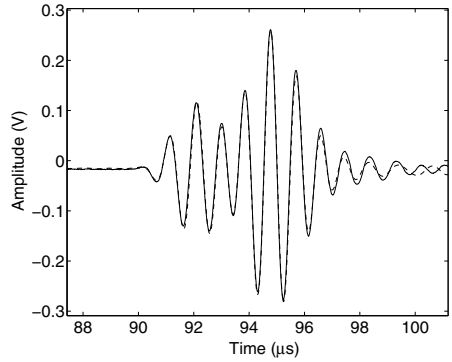

Figure 21. Comparison between the experimental transmitted signal (solid line) and the simulated transmitted signals (dashed line) using the reconstructed values of α_∞, ϕ, Λ, ν_b and E_b (sample M2).

21) reproduce correctly the experimental transmitted signals. This leads us to conclude that this method is well adapted for the characterization of cancellous bone.

Author details

Zine El Abiddine Fellah
LMA, CNRS, UPR 7051, Aix-Marseille Univ, Centrale Marseille, F-13402 Marseille Cedex 20, France

Mohamed Fellah
Laboratoire de Physique Théorique, Faculté de Physique, USTHB, BP 32 El Alia, Bab-Ezzouar, 16211, Alger- Algeria

Claude Depollier
Universite du Maine UMR CNRS 6613 Laboratoire d'Acoustique de l'Universite du Maine UFR STS Avenue O. Messiaen 72085 Le Mans CEDEX 09 France

LUNAM Universite du Maine. UMR CNRS 6613 Laboratoire d'Acoustique de l'Universite du MaineUFR STS Avenue O. Messiaen 72085 Le Mans CEDEX 09 France

4. References

[1] Allard JF (1993), Propagation of Sound in Porous Media : Modeling Sound Absorbing Materials, Chapman and Hall, London.
[2] Fellah ZEA, Depollier C (2000) Transient acoustic wave propagation in rigid porous media: A time domain approach, J. Acoust. Soc. Am. 107: (2), 683-688.
[3] Fellah ZEA, Depollier C, Fellah M, Lauriks W et Chpaleon JY (2005), Influence of dynamic tortuosity and compressibility on the propagation of transient waves in porous media, Wave Motion 41 (2): 145-161.
[4] Fellah ZEA, Fellah M, Lauriks W, Depollier C (2003), Direct inverse scattering of transient acoustic waves by a slab of rigid porous material., J. Acoust. Soc. Am. 113: (1) 61-72.
[5] Zwikker C, Kosten CW (1949) Sound Absorbing Materials, Elsevier , New York .
[6] Johnson D.L, Koplik J, Dashen R (1987) Theory of dynamic permeability and tortuosity in fluid-saturated porous media. J. Fluid. Mech. 176: 379-402.
[7] Allard JF, Champoux Y (1992), New empirical equations for sound propagation in rigid frame fibrous materials . Acoust. Soc. Am. 91: p. 3346.
[8] Champoux Y, Allard JF (1191), Dynamic tortuosity and bulk modulus in air-saturated porous media J. Appl. Phys. 70: p. 1975.
[9] Lafarge D, Lemarnier P, Allard JF, Tarnow V (1996), Dynamic compressibility of air in porous structures at audible frequencies Journ. Acoust. Soc. Am, 102: 4.
[10] Norris AN (1986), On the viscodynamic operator in Biot's equations of poroelasticity, J. Wave Mat. Interact. 1: 365-380.
[11] Pride SR, Morgan FD, Gangi AF (1993), Drag forces of porous media acoustics. Phys. Rev. B, 47: p. 4964.
[12] Szabo TL (1994), Time domain wave equations for lossy media obeying a frequency power law, J. Acoust. Soc. Am. 96: p. 491.
[13] Szabo TL (1995), Causal theories and data for acoustic attenuation obeying a frequency power law, Journal of the Acoustical Society of America 97: p. 14.
[14] Norton V, Novarini JC (2003), Including dispersion and attenuation directly in time domain for wave propagation in isotropic media, J. Acoust. Soc. Am. 113: p. 3024.
[15] Chen W, Holm S (2003), Modified Szabo's wave equation models for lossy media obeying frequency power law, J. Acoust. Soc. Am. 113: p. 3024.
[16] Samko SG, Kilbas AA, Marichev OI (1993), Fractional Integrals and Derivatives Theory and Applications, Gordon and Breach Publishers, Amsterdam.
[17] Abramowitz M, Stegun TA (1968), Handbook of mathematical functions, National bureau of standards, U.S. Governement Printing Office, Washington, DC. Chap. 6, p. 358.
[18] Fellah ZEA, Fellah M, Lauriks W, Depollier C, Angel Y, Chapelon JY (2003), Solution in time domain of ultrasonic propagation equation in porous material, Wave motion, 38: p. 151-163.

[19] Fellah ZEA, Depollier C, Fellah M (2001), Direct and inverse scattering problem in porous material having a rigid frame by fractional calculus based method, J. Sound. Vib. 244: (2), p. 359-366.
[20] Fellah ZEA, Ogam E, Wirgin A, Fellah M, Depollier C et Lauriks W, Ultrasonic characterization of porous materials: Inverse problem, J. Sound and Vib. 203:746-759.
[21] Leclaire P, Kelders L, Lauriks W, Glorieux C, Thoen J (1996), Determination of the viscous characteristic length in air-filled porous materials by ultrasonic attenuation measurements, J. Acoust. Soc. Am. 99: p. 1944.
[22] Ayrault C, Moussatov A, Castagnède B, Lafarge D, (1999) Ultrasonic characterization of plastic foams via measurements with static pressure variations, Applied Physics Letters 74: 3224.
[23] Moussatov A, Ayrault C, Castagnède B (2001), Porous material characterization ultrasonic method for estimation of tortuosity and characteristic length using a barometric chamber, Ultrasonic 39: 195.
[24] Leclaire P, Kelders L, Lauriks W, Brown NR, Melon M, Castagnède B (1996), Determination of viscous and thermal characteristic lengths of plastic foams by ultrasonic measurements in helium and air, J. Appl. Phys. 80:, p. 2009.
[25] Fellah ZEA, Depollier C, Berger S, Lauriks W, Trompette P, Chapelon JY (2003), Detemination of transport parameters in air saturated porous materials via ultrasonic reflected waves, J. Acoust. Soc. Am. 113: (5), 2561-2569.
[26] Fellah ZEA, Berger S, Lauriks W, Depollier C, Chapelon JY (2003), Inverse problem in air-saturated porous media via reflected waves, Rev. Sci. Inst. 74: (5), p. 2871.
[27] Fellah ZEA, Berger S, Lauriks W, Depollier C, Aristégui C, Chapelon JY (2003), Measuring the porosity and the tortuosity of porous materials via reflected waves at oblique incidence, J. Acoust. Soc. Am. 113: (5), p. 2424.
[28] Fellah ZEA, Berger S, Lauriks W, Depollier C, Trompette P, Chapelon JY (2003), Ultrasonic measuring of the porosity and tortuosity of air- saturated random packings of beads, J. Appl. Phys. 93: p. 9352.
[29] Fellah ZEA, Mitri FG, Depollier D, Berger S, Lauriks W Chapelon JY (2003), Characterization of porous materials having a rigid frame via reflected waves, J. Appl. Phys. 94: p. 7914.
[30] Fellah ZEA, Berger S, Lauriks W, Depollier C, Fellah M (2003), Measurement of the porosity of porous materials having a rigid frame via reflected waves : A time domain analysis with fractional derivatives, J. App. Phys, 93: p. 296.
[31] Fellah ZEA, Mitri FG, Fellah M, Ogam E, Depollier C (2007), Ultrasonic characterization of porous absorbing materials: Inverse problem, J. Sound. Vib. 302: 746-759.
[32] Fellah ZEA, Wirgin A, Fellah M, Sebaa N, Depollier C, Lauriks W (2005), A time-domain model of transient acoustic wave propagation in double-layered porous media, J. Acoust. Soc. Am. 118: 661-670.
[33] Fellah ZEA, Fellah M, Sebaa N, Lauriks W, Depollier C (2006) , Measuring flow resistivity of porous materials at low frequencies range via acoustic transmitted waves, J. Acoust. Soc. Am. 119: 1926-1928.
[34] Fellah ZEA, Fellah M, Mitri FG, Sebaa N, Lauriks W, Depollier C (2007), Transient acoustic wave propagation in air-saturated porous media at low frequencies, J. Appl. Phys. 102: 084906.
[35] Sebaa N, Fellah ZEA, Fellah M, Lauriks W, Depollier C (2005), Measuring flow resistivity of porous material via acoustic reflected waves, J. Appl. Phys. 98: 084901.

[36] Fellah ZEA, Fellah M, Mitri FG, Sebaa N, Depollier C, Lauriks W, Measuring permeability of porous materials at low frequency range via acoustic transmitted waves, Rev. Sci. Instrum. 78: 114902-10.
[37] Sadouki M, Fellah M, Fellah ZEA, Ogam E, Sebaa N, Mitri FG, Depollier C, Measuring static thermal permeability and inertial factor of rigid porous materials, J. Acoust. Soc. Am. 130: 2627-2630.
[38] Lagarias JC, Reeds JA, Wright MH, Wright PE (1998), Convergence properties of the Nedler-Mead Simplex Method in low dimensions SIAM J. Optim. 9: 112-147.
[39] Henry M, Allard JF (1997), Acoustical measurement of the trapping constant of foams with open cells, C. R. Acad. Sci. Paris 325: 331-338.
[40] Biot MA (1956), The theory of propagation of elastic waves in fluid-saturated porous solid. I. Low frequency range, J. Acoust. Soc. Am. 28: 168.
[41] Biot MA (1956), The theory of propagation of elastic waves in fluid-saturated porous solid. I. Higher frequency range, J. Acoust. Soc. Am. 28: 179.
[42] Fellah ZEA, Chapelon JY, Berger S, Lauriks W and Depollier C (2004), Ultrasonic wave propagation in human cancellous bone: Application of Biot theory, J. Acoust. Soc. Am. 116: (1), 61-73.
[43] Sebaa N, Fellah ZEA, Fellah M, Ogam E, Wirgin A, Mitri FG, Depollier C, Lauriks W (2006), Ultrasonic characterization of human cancellous bone using the Biot theory: Inverse problem, J. Acoust. Soc. Amer. 120: 1816-1824.
[44] Ogam E, Fellah ZEA, Sebaa N, Groby JP (2011), Non-ambiguous recovery of Biot poroelastic parameters of cellular panels using ultrasonic waves. J. Sound and Vibr. 330(6):1074-1090.
[45] Ogam E, Fellah ZEA (2011), The direct and inverse problems of an airsaturated poroelastic cylinder submitted to acoustic radiation. AipAdvances, 1(3):032174.
[46] Ogam E, Depollier C, Fellah ZEA (2010), The direct and inverse problems of an air-saturated porous cylinder submitted to acoustic radiation. Rev. Sci. Inst. 81(094902):9.
[47] Sebaa N, Fellah ZEA, Lauriks W, Depollier C (2006), Application of fractional calculus to ultrasonic wave propagation in human cancellous bone, Signal Processing 10: 2668-2677, DOI : 10.1016/j.sigpro.2006.02.015.
[48] Ashman RB, Rho JY (1988), Elastic modulus of trabecular bone material, J. Biomech. 21: 177-181.